JOURNAL OF GUIDANCE, CONTROL, AND DYNAMICS
Vol. 30, No. 1, January–February 2007

State-Dependent Riccati Equation Control for Small Autonomous Helicopters

Alexander Bogdanov*
Rockwell Scientific Company, Thousand Oaks, California 91360
and
Eric Wan†
Oregon Health & Science University, Beaverton, Oregon 97006

DOI: 10.2514/1.21910

This paper presents a flight control approach based on a state-dependent Riccati equation and its application to autonomous helicopters. For our experiments, we used two different platforms: an XCell-90 small hobby helicopter and a larger vehicle based on the Yamaha R-Max. The control design uses a six-degree-of-freedom nonlinear dynamic model that is manipulated into a *pseudolinear* form where system matrices are given explicitly as a function of the current state. A standard Riccati equation is then solved numerically at each step of a 50 Hz control loop to design the nonlinear state feedback control law online. In addition, the state-dependent Riccati equation control is augmented with a nonlinear compensator that addresses issues with the mismatch between the original nonlinear dynamics and its pseudolinear transformation.

Nomenclature

a_{mr}, a_{tr}	=	main and tail rotor blade lift curve slopes
a_1, b_1	=	longitudinal and lateral main rotor flapping angles
C_{Do}	=	rotor blade zero lift drag coefficient
$C_{\mathrm{La}}^{\mathrm{ht}}$, $C_{\mathrm{La}}^{\mathrm{vt}}$	=	horizontal and vertical tail lift curve slopes
C_T	=	rotor thrust coefficient
c_{mr}, c_{tr}	=	main and tail rotor chords
h_{mr}	=	main rotor hub height above the center of gravity
$\mathbf{I}$	=	helicopter inertia matrix
I_{xx}, I_{yy}, I_{zz}	=	main moments of inertia
$I_{\beta\mathrm{mr}}$	=	main rotor blade moment of inertia
K_i, K_p	=	integral and proportional gains of the engine speed governor
K_{lon}, K_{lat}	=	longitudinal and lateral cyclic control to flap gains
K_β	=	main rotor hub torsional stiffness
K_λ	=	rotor wake intensity factor
K_μ	=	scaling factor of flap response to speed variation
L, M, N	=	rolling, pitching, and yawing moments
m	=	helicopter mass
n_{tr}	=	gear ratio between main and tail rotors
$\mathbf{P}$	=	solution of the algebraic Riccati equation
P_e	=	engine power
p, q, r	=	vehicle angular (roll, pitch, and yaw) rates
$\mathbf{Q}$, $\mathbf{R}$	=	state and control cost matrices in the state-dependent Riccati equation design
Q_e	=	engine torque
R_{mr}, R_{tr}	=	main and tail rotor radii
S_{ht}, S_{vt}	=	horizontal and vertical tail areas
S_{mr}, S_{tr}	=	main and tail rotor disk areas
S_x^{fus}, S_y^{fus}, S_z^{fus}	=	frontal, side, and vertical fuselage drag area
T_{mr}, T_{tr}	=	main and tail rotor thrust
u, v, w	=	vehicle velocities along x, y, and z fuselage axes
$\boldsymbol{u}$	=	helicopter control vector
u_{col}, u_{tcol}	=	main and tail rotors collective control inputs
u_{lon}, u_{lat}	=	longitudinal and lateral cyclic control inputs
$\boldsymbol{u}^{\mathrm{sd}}$, $\boldsymbol{u}^c$	=	state-dependent Riccati equation control and compensator output
u_w, v_w, w_w	=	wind velocities along x, y, and z fuselage axes
V_{imr}, V_{itr}	=	main and tail rotor-induced velocities
V_{tip}	=	speed of the rotor blade tip
V_∞	=	total fuselage air speed
V_∞^{vt}	=	vertical tail axial velocity
$\boldsymbol{w}$	=	vector of wind velocities u_w, v_w, w_w
X, Y, Z	=	forces along x, y, and z fuselage axes
$\boldsymbol{x}$	=	helicopter state vector
x, y, z	=	vehicle position in inertial frame
x_{ht}	=	horizontal tail offset from the center of gravity along x axis
x_{tr}	=	tail rotor hub offset from the center of gravity along x axis
x_{vt}	=	vertical tail offset from the center of gravity along x axis
z_{tr}	=	tail rotor hub offset from the center of gravity along z axis
z_{vt}	=	vertical tail offset from the center of gravity along z axis
γ_{fb}	=	stabilizer bar Lock number
$\delta_{\mathrm{tr}}^{\mathrm{trim}}$	=	tail rotor pitch offset
$\epsilon_{\mathrm{vt}}^{\mathrm{tr}}$	=	fraction of the vertical tail exposed to the tail rotor downwash
η_w	=	coefficient of nonideal main rotor wake contraction
λ_0	=	main rotor inflow ratio in steady state
μ	=	advance ratio
μ_z	=	normal airflow component
ρ	=	air density
σ	=	rotor solidity ratio
τ_{fb}	=	time constant of a rotor with a stabilizer bar
τ_λ	=	main rotor inflow time constant
ϕ, θ, ψ	=	Euler angles of roll, pitch, and yaw
Ω_{mr}, Ω_{tr}	=	main and tail rotor speeds

Received 19 December 2005; revision received 23 March 2006; accepted for publication 13 April 2006.

*Research Scientist, Department of Interactive and Autonomous Systems; abogdanov@rwsc.com. AIAA member.

†Associate Professor, Department of Computer Science and Electrical Engineering, OGI School of Science and Engineering; ericwan@csee.ogi.edu. AIAA member.

Subscripts

fus	=	fuselage
ht	=	horizontal tail
mr	=	main rotor
tr	=	tail rotor
vt	=	vertical tail

Introduction

AUTONOMOUS flight control systems for helicopters present significant challenges due to their highly nonlinear and unstable nature. A number of previously demonstrated designs vary from linear robust control laws [1,2] to nonlinear algorithms, examples of which include approximate feedback linearization [2] and neural network adaptive control [3]. In this paper, we develop a nonlinear controller capable of autonomous operations through a broad spectrum of maneuvers by employing another technique that has shown considerable promise. The design involves manipulating the system dynamic equations into a pseudolinear or state-dependent coefficient (SDC) form, in which system matrices are given explicitly as a function of the current state. Treating the system matrices as constant for the current time step, the approximate solution of the nonlinear state-dependent Riccati equation (SDRE) is obtained online for the reformulated SDC dynamical system. The solution is then used to calculate a feedback control law that is optimized around the system state estimated at each time step. This technique, referred to as state-dependent Riccati equation (SDRE) control [4], provides an approximate solution for the optimal control problem with a linear quadratic (LQ) cost function.

The SDRE control approach has received considerable attention in recent years. Stability properties are discussed in [4–7], controllability issues are studied in [8], and a power series formulation was used in [9] to deal with control nonlinearities. A review of SDRE-based control and estimation can also be found in [10]. In practice, SDRE has been successfully demonstrated in such applications as attitude control of a satellite [11] and a spacecraft [12], missile autopilot design [13–15], and underactuated robot control [16]. Our work in this area was first motivated by experiments with a double inverted pendulum on a cart [17]. We then applied the SDRE approach to helicopter control in a model predictive control framework where the SDRE was used to generate an initial control solution, which then was further refined numerically [18]. The computational load of that approach, however, appeared prohibitive for practical implementation on our current onboard hardware. This paper uses only the SDRE control and provides a complete derivation of the state-dependent equations necessary for small helicopter dynamics.

An additional contribution in this paper includes an *augmented* SDRE formulation. We show that direct application of the SDRE technique to a helicopter model results in the necessity to further simplify the vehicle model due to a number of terms that cannot be effectively presented in the SDC form. This results in a model mismatch between the original nonlinear dynamics and the transformed model used in the SDRE design. To overcome this problem, we augment the SDRE feedback control with a nonlinear compensator that approximately cancels the differences between the original model and the model used in the SDRE design. The augmentation provides an approximate match of the vehicle response to the one of the SDC model used by the SDRE. It also provides a reference input for tracking purposes and replaces simple fixed "trim" control that is usually added to ensure altitude and heading hold in hover or level flight.

We also demonstrate real-time feasibility of the designed control. The SDRE technique is often associated with a high computational load as it involves solving an algebraic Riccati equation at each time step. To ensure real-time computation of the SDRE solution, we use a simple iterative algorithm that enables an efficient computational performance.

In this paper, we use a nonlinear dynamic model of a helicopter originally described in [19]. The model consists of a six-degree-of-freedom (6-DOF) rigid body model augmented with simplified nonlinear models of the rotor torque and thrust, rotor flapping dynamics, and aerodynamic forces and moments. We present results of our work obtained from both simulations and flight tests on an instrumented XCell-90 small-scale acrobatic radio controlled helicopter and a second larger vehicle based on the Yamaha R-Max.

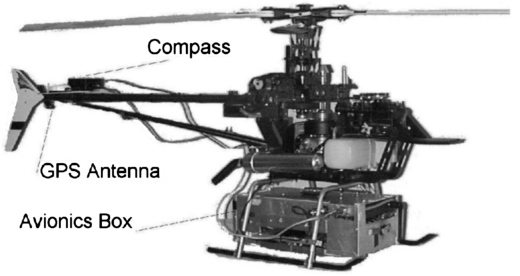

Fig. 1 XCell-90 helicopter with sensors and avionics box.

Fig. 2 Yamaha R-Max helicopter (GTMAX).

The paper is organized as follows: The first section describes the two experimental helicopters used in our work. In the next section, we start with a brief overview of the augmented SDRE approach followed by a description of a generic model of a small-size helicopter with a hingeless rotor. The SDRE approach is then applied to the helicopter model, and a compensator is designed to mitigate effects of the approximate SDC parameterization and provide reference (trim control) input. The last section of the paper presents experimental results obtained from simulations and real test flights.

Experimental Vehicles

Our XCell-90 helicopter and avionics (Fig. 1) is a clone of a Massachusetts Institute of Technology (MIT) research vehicle [20]. The hobby vehicle is a small-scale model weighing only 8 kg and features a 0.9 $in.^3$ engine with an external standalone speed governor, clockwise rotating main rotor (diameter is 1.5 m) with a hingeless rotor hub, and a Bell–Hiller teetering stabilizer bar. Both main and tail rotor blades, as well as the stabilizer bar, have symmetric airfoils. The custom avionics package weighs 3 kg and includes an Inertial Sciences ISIS inertial measurement unit (IMU) with three angular rate gyroscopes and three accelerometers, a 10 Hz global positioning system (GPS) receiver, a barometric altimeter, wireless communications, and an onboard PC-104 computer based on the Geode GX1 300 MHz microprocessor running the QNX-4 operating system.

The second helicopter (Fig. 2) is the GTMAX: a larger vehicle developed at the Georgia Institute of Technology (GATech) [21]. The GTMAX is based on the Yamaha R-Max industrial helicopter airframe, which was designed as an unmanned vehicle to distribute agricultural chemicals over farm crops. The R-Max is capable of carrying a payload of over 30 kg; it is equipped with a 21 hp gasoline engine, generator, and battery, and has an electric starter. The GTMAX avionics package weighs about 16 kg and includes general purpose processing capabilities and sensing: two embedded PCs (266 MHz and 850 MHz), an ISIS IMU, a NovAtel RT-2 differential GPS, a three-axis magnetometer, a sonar altimeter, a radar altimeter,

Table 1 XCell-90 and GTMAX model parameters

Parameter	XCell	GTMAX	Description
a_{mr}, rad^{-1}	5.50	5.73	Main rotor blade lift curve slope
a_{tr}, rad^{-1}	5.0	5.0	Tail rotor blade lift curve slope
C_{D0}^{mr}	0.024	0.01	Main rotor blade zero lift drag coefficient
C_{D0}^{tr}	0.024	0.01	Tail rotor blade zero lift drag coefficient
$C_{\mathrm{La}}^{\mathrm{ht}}$, rad^{-1}	2.0	N/A	Horizontal tail lift curve slope
$C_{\mathrm{La}}^{\mathrm{vt}}$, rad^{-1}	2.0	N/A	Vertical tail lift curve slope
c_{mr}, m	0.058	0.131	Main rotor chord
$C_{T\max}^{\mathrm{mr}}$	0.0055	N/A	Main rotor maximum thrust coefficient
$C_{T\max}^{\mathrm{tr}}$	0.05	N/A	Tail rotor maximum thrust coefficient
c_{tr}, m	0.029	0.047	Tail rotor chord
h_{mr}, m	0.305	0.438	Main rotor hub height above center of gravity
I_{xx}, kg $\cdot$ m^2	0.180	3.246	Rolling moment of inertia
I_{yy}, kg $\cdot$ m^2	0.340	11.229	Pitching moment of inertia
I_{zz}, kg $\cdot$ m^2	0.280	9.856	Yawing moment of inertia
$I_{\beta\mathrm{mr}}$, kg $\cdot$ m^2	0.038	1.420	Main rotor blade flapping inertia
K_i	0.01	N/A	Integral engine governor gain
K_{lat}	4.20	2.51	Lateral cyclic-to-flap gain at nominal rotor speed
K_{lon}	4.20	2.51	Longitudinal cyclic-to-flap gain at nominal rotor speed
K_p	0.02	N/A	Proportional engine governor gain
K_β, N $\cdot$ m	54.0	661.4	Main rotor hub torsional stiffness
K_μ	0.2	N/A	Speed to flap coefficient
m, kg	8.0	74	Helicopter mass
n_{tr}	5.54	6.71	Gear ratio between tail and main rotors
$P_e^{\max}$, W	2000	15660	Engine maximum power
R_{mr}, m	0.775	1.555	Main rotor radius
R_{tr}, m	0.130	0.273	Tail rotor radius
S_{ht}, m^2	0.0086	N/A	Effective horizontal tail area
S_{vt}, m^2	0.0135	N/A	Effective vertical tail area
S_x^{fus}, m^2	0.10	0.74	Frontal fuselage area
S_y^{fus}, m^2	0.22	0.74	Side fuselage area
S_z^{fus}, m^2	0.15	0.74	Vertical fuselage area
x_{ht}, m	−0.650	−0.775	Horizontal tail offset from center of gravity along the x axis
x_{tr}, m	−0.93	−1.84	Tail rotor hub offset from center of gravity along the x axis
x_{vt}, m	−0.92	−1.88	Vertical tail offset from center of gravity along the x axis
z_{tr}, m	−0.115	−0.144	Tail rotor hub offset from center of gravity along the z axis
z_{tr}, m	−0.095	−0.236	Vertical tail offset from center of gravity along the z axis
γ_{fb}	0.8	0.2	Stabilizer bar Lock number
$\delta_{\mathrm{tr}}^{\mathrm{trim}}$	0.185	0.150	Tail rotor pitch offset
$\epsilon_{\mathrm{vt}}^{\mathrm{tr}}$	0.2	N/A	Fraction of vertical tail exposed to tail rotor downwash
$\Omega_{\mathrm{mr}}^{\mathrm{nom}}$, rad/s	167	89	Nominal main rotor speed

and wireless telemetry. Servo commands are given as raw data via a modified Yamaha attitude control system (YACS) interface. Controlling the actuators through the YACS results in a 180–200 ms delay in the 50 Hz control loop, which is equal to 9 or 10 control cycles and represents an additional challenge in control design. GATech's GTMAX mathematical model is based on the same principles as MIT's approach, yet it is slightly different as it accounts for main rotor blade twist, has a simple ground effect, rotor thrust is limited only by the collective blade pitch, and main rotor and stabilizer bar flapping dynamics are not aggregated into one. The GTMAX does not have an integrated engine governor, and the control algorithm has to incorporate engine speed control. For the reader's convenience, the XCell-90 and GTMAX model parameters are presented in Table 1. Parameters specific to the XCell-90 are marked as "not applicable" (N/A) for the GTMAX model.

For brevity, this paper focuses on the XCell-90 model for detailing the control design and performance analysis in simulation. Adapting the control design to the GTMAX requires only minor modifications and substitutions of parameters. Actual flight results are presented for both helicopters.

Control Design

Brief Overview

The SDRE approach [4] is based on *extended linearization* of the vehicle dynamics that involves manipulating the dynamic equations

$$\dot{\boldsymbol{x}} = \boldsymbol{f}(\boldsymbol{x}, \boldsymbol{u}) \tag{1}$$

into a control-affine SDC form with state vector $\boldsymbol{x}$ and control $\boldsymbol{u}$, in which system matrices are explicit functions of the current state

$$\dot{\boldsymbol{x}} = \mathbf{A}(\boldsymbol{x})\boldsymbol{x} + \mathbf{B}(\boldsymbol{x})\boldsymbol{x} \tag{2}$$

As a trivial example, consider $\dot{x} = \sin x + \cos xu$, then $A(x) = (\sin x)/x$, $B(x) = \cos x$. SDC parameterization is not unique. Consider $\mathbf{f}(\boldsymbol{x}) = \mathbf{A}(\boldsymbol{x})\boldsymbol{x}$, in which case $\mathbf{f}(\boldsymbol{x}) = [\mathbf{A}(\boldsymbol{x}) + \mathbf{E}(\boldsymbol{x})]\boldsymbol{x}$ for any matrix that satisfies $\mathbf{E}(\boldsymbol{x})\boldsymbol{x} = 0$. The nonuniqueness can affect controllability of the parameterized pair $(\mathbf{A}(\boldsymbol{x}), \mathbf{B}(\boldsymbol{x}))$. Note, however, that controllability of the original dynamics is not guaranteed by this condition alone [8].

If the pair $(\mathbf{A}(\boldsymbol{x}), \mathbf{B}(\boldsymbol{x}))$ is pointwise controllable, then linear system methods can be applied to design a state feedback control, e.g., $\boldsymbol{u} = -\mathbf{K}(\boldsymbol{x})\boldsymbol{x}$, that provides $\mathbf{A}_c(\boldsymbol{x}) \equiv \mathbf{A}(\boldsymbol{x}) - \mathbf{B}(\boldsymbol{x})\mathbf{K}(\boldsymbol{x}) < 0$. Generally, only local asymptotic stability of the original system is guaranteed without additional conditions. Results from linear time-varying systems theory can be applied to determine stability properties [22].

The SDRE design employs an online solution of the standard Riccati equation to compute the optimal feedback gain matrix $\mathbf{K}(\boldsymbol{x})$, corresponding to the local solution of the LQ optimal control problem. The SDRE thus approximates a solution to the LQ optimal control problem

$$\boldsymbol{u} = \arg\ \min\left\{\int_t^\infty (\boldsymbol{x}^T\mathbf{Q}\boldsymbol{x} + \boldsymbol{u}^T\mathbf{R}\boldsymbol{u})\,\mathrm{d}\tau\right\}$$

subject to (1) and (2) by solving the LQR problem at each t for the linear time-invariant system $\mathbf{A} = \mathbf{A}(\boldsymbol{x}(t))$ and $\mathbf{B} = \mathbf{B}(\boldsymbol{x}(t))$, which

yields an exact solution to the problem assuming fixed $\mathbf{A}(\boldsymbol{x})$ and $\mathbf{B}(\boldsymbol{x})$ for time $[t, \infty)$.

The SDRE gain scheduling is similar to the linear parameter varying (LPV) framework [23,24]. In the LPV structure, the coefficient matrices are functions of a parameter, whereas in the SDC structure, the coefficient matrices are functions of the state. The LPV control is designed to stabilize a system throughout the whole range of the parameter values, whereas SDRE design is based on the LQ cost function minimization.

The SDRE control generally exhibits greater stability and better performance than linear control laws (e.g., LQR), and empirical experience often shows that in many cases the domain of attraction is as large as the domain of interest [4,17].

For digital implementation purposes, we discretize $\mathbf{A}(\boldsymbol{x})$, $\mathbf{B}(\boldsymbol{x})$ into $\mathbf{\Phi}(\boldsymbol{x}_k)$, $\Gamma(\boldsymbol{x}_k)$ at every sampling interval and then compute the digital tracking control

$$\boldsymbol{u}_k = -\mathbf{R}^{-1}\Gamma^T(\boldsymbol{x})\mathbf{P}(\boldsymbol{x}_k)\left(\boldsymbol{x}_k - \boldsymbol{x}_k^{\text{des}}\right) + \boldsymbol{u}_{\text{ref}} \equiv -\mathbf{K}(\boldsymbol{x}_k)\boldsymbol{e}_k + \boldsymbol{u}_{\text{ref}}$$

where $\boldsymbol{x}_k^{\text{des}}$ is a desired state, $\boldsymbol{u}_{\text{ref}}$ is a reference input (trim control), and $\mathbf{P}(\boldsymbol{x}_k)$ is the solution of the discrete-time algebraic Riccati equation (DARE)

$$\mathbf{\Phi}^T[\mathbf{P} - \mathbf{P}\Gamma(\mathbf{R} + \Gamma^T\mathbf{P}\Gamma)^{-1}\Gamma^T\mathbf{P}]\mathbf{\Phi} - \mathbf{P} + \mathbf{Q} = 0 \tag{3}$$

using state-dependent matrices $\mathbf{\Phi}(\boldsymbol{x}_k)$ and $\Gamma(\boldsymbol{x}_k)$, which are treated as being constant at each time step.

Real-time computation of the SDRE control algorithm at 50 Hz using the onboard computer demands a computationally efficient algorithm to find the SDRE gain matrix. For single input systems, Erdem and Alleyne [16] computed SDRE gain values by finding stable eigenvalues of the Hamiltonian matrix (closed-loop system poles) and then employing pole placement to compute the gains via Ackerman's formula. This method, however, becomes inefficient for higher order multi-input systems, which require additional eigenvector computations. Generally, a numeric solution of the DARE is necessary. Kleinman's iterative algorithm is often cited as a fast method to solve the *continuous* algebraic Riccati equation [25]. Our approach, however, was to use a direct iterative propagation of the difference Riccati equation:

$$\mathbf{P}_k = \mathbf{\Phi}^T(\mathbf{P}_{k+1} - \mathbf{P}_{k+1}\Gamma(\mathbf{R} + \Gamma^T\mathbf{P}_{k+1}\Gamma)^{-1}\Gamma^T\mathbf{P}_{k+1}]\mathbf{\Phi} + \mathbf{Q}$$

By seeding $\mathbf{P}_N$ with the solution from the previous sampling interval, only a few iterations (less than 10) appeared to be necessary for convergence to an approximate solution with sufficient accuracy to calculate the control. With the 300 MHz Geode GX1 processor on the XCell-90, we were able to calculate an SDRE control law using a 12-element state vector in approximately 14 ms. This processor also handles sensor inputs, state estimation, and data logging within the same 20 ms time frame, providing control at a 50 Hz rate.

SDC reformulation of the nonlinear dynamic equations specific to the helicopter model does not yield an exact parameterization as in Eq. (2) due to various nonparameterizable terms in the original dynamics and the fact that the helicopter model is not linear with respect to the controls. This results in an additional term $\Delta\boldsymbol{f}(\boldsymbol{x}, \boldsymbol{u})$ characterizing a mismatch between the original dynamics and its SDC parameterization:

$$\boldsymbol{f}(\boldsymbol{x}, \boldsymbol{u}) = \mathbf{A}(\boldsymbol{x})\boldsymbol{x} + \mathbf{B}(\boldsymbol{x})\boldsymbol{u} + \Delta\boldsymbol{f}(\boldsymbol{x}, \boldsymbol{u})$$

In this case, one may expect the dynamic response of the actual and approximated systems to differ. To overcome this problem, the control design is modified to include an additive correction term: $\boldsymbol{u} = \boldsymbol{u}^{\text{sd}} + \boldsymbol{u}^c$ (see Fig. 3), i.e., we augment the SDRE control $\boldsymbol{u}^{\text{sd}}$ with a nonlinear compensator $\boldsymbol{u}^c$ that provides *model matching* and additionally serves as a *reference input* (trim control) for tracking:

$$\boldsymbol{f}(\boldsymbol{x}, \boldsymbol{u}^{\text{sd}} + \boldsymbol{u}^c) - \dot{\boldsymbol{x}}_{\text{des}} \approx \mathbf{A}(\boldsymbol{x})\boldsymbol{e} + \mathbf{B}(\boldsymbol{x})\boldsymbol{u}^{\text{sd}} \tag{4}$$

The purpose of the compensator is thus to (approximately) cancel the term $\Delta\boldsymbol{f}(\boldsymbol{x}, \boldsymbol{u})$. This matches the vehicle dynamics (1) to the reference SDRE dynamics (2) and provides performance close to the potential of the ideal SDRE design.

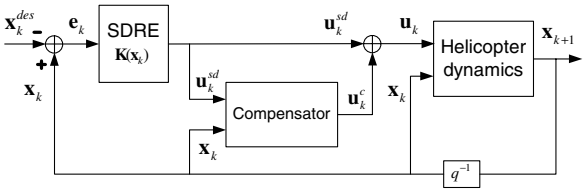

Fig. 3 Augmented SDRE control diagram.

One may notice certain similarities between the compensator idea and feedback linearization. In general, feedback linearization shapes the system dynamics to provide a desired response through a nonlinear state transformation and state error feedback. The nonlinear coordinate transformation renders a new state space where the original dynamics are described by linear equations. A linear control law is then applied to provide the desired response (e.g., pole placement) [26]. In a trivial case, where the input matrix is nonsingular everywhere, simple inversion can be done without explicit coordinate transformation. In our case of the augmented SDRE, only a *part* of the system that is not presentable in the SDC form needs to be inverted, and the SDRE control provides the desired dynamic response. Although feedback linearization criteria are known [26], we did not investigate general criteria of applicability of the augmented SDRE control. Although certain assumptions were necessary to derive the compensator in this paper, similar assumptions are also required for static feedback linearization of a generic helicopter model [2].

In the following sections, we detail the SDC formulation for the SDRE design and the specifics of the compensator for the helicopter model.

Helicopter Model

The helicopter dynamics as used in the simulator are described as a 6-DOF rigid body model with translational velocities $\boldsymbol{v} = (u, v, w)^T$, angular velocities $\boldsymbol{\omega} = (p, q, r)^T$, Euler angles $\boldsymbol{q} = (\phi, \theta, \psi)^T$, position of the center of mass $\boldsymbol{p} = (x, y, z)^T$, 3×3 inertia matrix $\mathbf{I}$, and mass m. The rigid body moves under influence of external forces $\boldsymbol{F} = (X, Y, Z)^T = \boldsymbol{F}_{\text{mr}} + \boldsymbol{F}_{\text{tr}} + \boldsymbol{F}_g + \boldsymbol{F}_{\text{vt}} + \boldsymbol{F}_{\text{ht}} + \boldsymbol{F}_{\text{fus}}$ and moments $\boldsymbol{M} = (L, M, N)^T = \boldsymbol{M}_{\text{mr}} + \boldsymbol{M}_{\text{tr}} + \boldsymbol{M}_e + \boldsymbol{M}_{\text{vt}} + \boldsymbol{M}_{\text{ht}}$ originating from the main and tail rotors, engine, gravity, vertical and horizontal tails, and fuselage drag (we assume that the fuselage center of pressure coincides with the center of mass, and thus no moments arise from the fuselage drag). The dynamic model can be summarized as

$$\begin{gathered}\dot{\boldsymbol{v}} = -\boldsymbol{\omega} \times \boldsymbol{v} + \frac{1}{m}\boldsymbol{F}, \qquad \dot{\boldsymbol{\omega}} = -\mathbf{I}^{-1}\boldsymbol{\omega} \times \mathbf{I}\boldsymbol{\omega} + \mathbf{I}^{-1}\boldsymbol{M} \\ \dot{\boldsymbol{q}} = \mathbf{\Psi}(\boldsymbol{q})\boldsymbol{\omega}, \qquad \dot{\boldsymbol{p}} = \mathbf{R}(\boldsymbol{q})\boldsymbol{v}\end{gathered} \tag{5}$$

where $\mathbf{R}(\boldsymbol{q}) \in SO(3)$ is a linear velocity transformation matrix and $\mathbf{\Psi}(\boldsymbol{q})$ describes angular velocity transformation

$$\mathbf{R} = \begin{pmatrix} c\theta c\psi & -c\phi s\psi + s\phi s\theta c\psi & s\phi s\psi + c\phi s\theta c\psi \\ c\theta s\psi & c\phi c\psi + s\phi s\theta s\psi & -s\phi c\psi + c\phi s\theta s\psi \\ -s\theta & s\phi c\theta & c\phi c\theta \end{pmatrix}$$

$$\mathbf{\Psi} = \begin{pmatrix} 1 & s\phi t\theta & c\phi t\theta \\ 0 & c\phi & -s\phi \\ 0 & s\phi/c\theta & c\phi/c\theta \end{pmatrix}$$

with "s," "c," and "t" standing for "sin," "cos," and "tan," respectively.

Four control inputs $\boldsymbol{u} = (u_{\text{lon}}, u_{\text{lat}}, u_{\text{col}}, u_{\text{tcol}})^T$ affect tilting moments of the main rotor in the longitudinal and lateral directions (M_{mr} and L_{mr}), main rotor thrust, and tail rotor thrust (T_{mr} and T_{tr}). Main and tail rotor collective inputs u_{col} and u_{tcol} simultaneously change pitch of all the rotor blades, thus regulating the main and tail rotor thrust magnitude. Longitudinal and lateral cyclic inputs u_{lon} and

u_{lat} control pitch of the rotor blades as a function of their azimuth angles, thus creating differential lift on the front–aft, and left–right blades. This causes the blades to flap, which results in longitudinal and lateral moments in the rotor hub and also deflects the total thrust vector from the direction of the rotor shaft. The main rotor and stabilizer bar flapping dynamics is lumped and represented by tip-path plane flapping dynamics with only two states a_1 and b_1 and a time constant $\tau_{\text{fb}} = 16(\gamma_{\text{fb}}\Omega_{\text{mr}})^{-1}$ that depends on the stabilizer bar Lock number and rotor speed [19]:

$$\dot{a}_1 = -q - \frac{a_1}{\tau_{\text{fb}}} + \frac{1}{\tau_{\text{fb}}}\left(\frac{\partial a_1}{\partial \mu}\frac{u-u_w}{V_{\text{tip}}} + \frac{\partial a_1}{\partial \mu_z}\frac{w-w_w}{V_{\text{tip}}}\right) + \frac{K_{\text{lon}}}{\tau_{\text{fb}}}u_{\text{lon}} \tag{6}$$

$$\dot{b}_1 = -p - \frac{b_1}{\tau_{\text{fb}}} + \frac{1}{\tau_{\text{fb}}}\frac{\partial b_1}{\partial \mu_v}\frac{v-v_w}{V_{\text{tip}}} + \frac{K_{\text{lat}}}{\tau_{\text{fb}}}u_{\text{lat}} \tag{7}$$

where flapping derivatives $\partial a_1/\partial \mu = -\partial b_1/\partial \mu_v$.

For further reference, we provide brief expressions for the forces and moments in the helicopter model (additional details are available in [19,27]). The main rotor forces are induced by the rotor thrust and rotor plane deflection due to flapping; the moments have an additional component due to the stiffness of the blade–hub assembly:

$$X_{\text{mr}} = -\sin(a_1)T_{\text{mr}} \tag{8}$$

$$Y_{\text{mr}} = \sin(b_1)T_{\text{mr}} \tag{9}$$

$$Z_{\text{mr}} = -T_{\text{mr}} \tag{10}$$

$$L_{\text{mr}} = \sin(b_1)(h_{\text{mr}}T_{\text{mr}} + K_\beta) \tag{11}$$

$$M_{\text{mr}} = \sin(a_1)(h_{\text{mr}}T_{\text{mr}} + K_\beta) \tag{12}$$

where the rotor thrust computation $T_{\text{mr}} = C_T\rho V_{\text{tip}}^2 S_{\text{mr}}$ is based on the momentum theory, assuming *steady and uniform* inflow. According to [27], the time constant for inflow transients at hover is $\tau_\lambda = 0.849/(4\lambda_h\Omega_{\text{mr}})^{-1}$, where the inflow ratio in hover $\lambda_h = V_{\text{imr}}/V_{\text{mr}}^{\text{tip}} = \sqrt{mg/(2\rho\pi R_{\text{mr}}^2)}/(\Omega_{\text{mr}}R_{\text{mr}})$. For the XCell-90, as estimated in [19], $\tau_\lambda \approx 0.038$ s; for the GTMAX, the formula yields $\tau_\lambda \approx 0.053$ s, which in both cases is significantly faster than the rigid body dynamics. During the maneuvers requiring large thrust variations, the time constant may change substantially. However, high rotor hub torsional stiffness that dominates cyclic authority in small-size helicopters with hingeless rotors, as with the XCell [19], makes modeling of the inflow transients less critical. With such an assumption, thrust computation involves a numerical solution of a system of nonlinear equations for the thrust coefficient and inflow ratio in steady state:

$$C_T = \frac{a_{\text{mr}}\sigma}{2}\left[u_{\text{col}}\left(\frac{1}{3} + \frac{\mu^2}{2}\right) + \frac{\mu_z - \lambda_0}{2}\right] \tag{13}$$

$$\lambda_0 = \frac{C_T}{2\eta_w\sqrt{\mu^2 + (\lambda_0 - \mu_z)^2}} \tag{14}$$

Because the main rotor is flexibly connected to the fuselage through the engine, the yawing moment is produced by the engine ($N_e = -Q_e$), which is described as a first-order nonlinear ordinary differential equation:

$$\dot{\Omega}_{\text{mr}} = \dot{r} + \frac{1}{I_{\text{rot}}}(Q_e - Q_{\text{mr}} - n_{\text{tr}}Q_{\text{tr}}) \tag{15}$$

where $I_{\text{rot}} \approx 2.5I_{\beta\text{mr}}$ is inertia of the rotor assembly (two main rotor blades and other rotating parts). The engine torque is proportional to the throttle input $Q_e = (P_e^{\max}/\Omega_{\text{mr}})u_{\text{thr}}$, and the main rotor torque is modeled as a sum of induced drag and profile drag (the tail rotor torque similarly):

$$Q_{\text{mr}} = T_{\text{mr}}R_{\text{mr}}(\lambda_0 - \mu_z) + \frac{C_{D0}\sigma}{8}\left(1 + \frac{7}{3}\mu^2\right)\rho V_{\text{tip}}^2 S_{\text{mr}}R_{\text{mr}} \tag{16}$$

The tail rotor forces and moments are induced by the tail rotor thrust, which is computed similarly to the main rotor thrust,

$$Y_{\text{tr}} = -T_{\text{tr}} \tag{17}$$

$$L_{\text{tr}} = z_{\text{tr}}T_{\text{tr}} \tag{18}$$

$$M_{\text{tr}} = Q_{\text{tr}} \tag{19}$$

$$N_{\text{tr}} = -x_{\text{tr}}T_{\text{tr}} \tag{20}$$

As the empennage glides through the air, it generates aerodynamic lift and drag. The vertical tail forces and moments are given by

$$Y_{\text{vt}} = 0.5\rho S_{\text{vt}}\left(C_{\text{La}}^{\text{vt}}V_\infty^{\text{vt}} + |v_{\text{vt}}|\right)v_{\text{vt}} \tag{21}$$

$$L_{\text{vt}} = -z_{\text{vt}}Y_{\text{vt}} \tag{22}$$

$$N_{\text{vt}} = x_{\text{vt}}Y_{\text{vt}} \tag{23}$$

where the axial velocity of the tail $V_\infty^{\text{vt}} = \sqrt{(u-u_w)^2 + (w - w_w + |x_{\text{vt}}|q - K_\lambda V_{\text{imr}})^2}$ and the normal velocity $v_{\text{vt}} = v - v_w + x_{\text{vt}}r - \epsilon_{\text{vt}}^{\text{tr}}V_{\text{itr}}$. Wake intensity factor K_λ is calculated as a function of the forward velocity. The horizontal tail forces and moments are expressed as

$$Z_{\text{ht}} = 0.5\rho S_{\text{ht}}\left(C_{La}^{\text{ht}}|u - u_w| + |w_{\text{ht}}|\right)w_{\text{ht}} \tag{24}$$

$$M_{\text{ht}} = -x_{\text{ht}}Z_{\text{ht}} \tag{25}$$

where effective vertical speed $w_{\text{ht}} = w_w - x_{\text{ht}}q - K_\lambda V_{\text{imr}}$.

Fuselage drag is described as a drag of a flat plate exposed to dynamic pressure:

$$V_\infty = \sqrt{(u-u_w)^2 + (v-v_w)^2 + (w - w_w + V_{\text{imr}})^2} \tag{26}$$

$$X_{\text{fus}} = -0.5\rho S_x^{\text{fus}}V_\infty(u - u_w) \tag{27}$$

$$Y_{\text{fus}} = -0.5\rho S_y^{\text{fus}}V_\infty(v - v_w) \tag{28}$$

$$Z_{\text{fus}} = -0.5\rho S_z^{\text{fus}}V_\infty(w - w_w + V_{\text{imr}}) \tag{29}$$

Neglecting the actuators' dynamics, the helicopter model is thus described by a 15th-order system of differential equations, with a state vector defined as $\boldsymbol{x}_h = (\boldsymbol{v}, \boldsymbol{\omega}, \boldsymbol{q}, \boldsymbol{p}, a_1, b_1, \Omega_{\text{mr}})$. The model is considered suitable for a class of miniature helicopters with hingeless rotors [19]. In the following, we assume an external engine governor and do not treat the throttle as a control input.

State-Dependent Formulation for the Helicopter Model

For control design, we define the observable states to correspond to the standard 12 state variables of a 6-DOF rigid body model $\boldsymbol{x} = (\boldsymbol{v}, \boldsymbol{\omega}, \boldsymbol{q}, \boldsymbol{p}) \equiv (u, v, w, p, q, r, \phi, \theta, \psi, x, y, z)^T$. We further assume an external engine governor and approximate the main rotor flapping in steady state:

$$b_1(\boldsymbol{x}, \boldsymbol{w}, u_{\text{lat}}) = -\tau_{\text{fb}}p + \frac{\partial b_1}{\partial \mu_v}\frac{v - v_w}{V_{\text{tip}}} + K_{\text{lat}}u_{\text{lat}} \tag{30}$$

$$a_1(\boldsymbol{x}, \boldsymbol{w}, u_{\text{lon}}) = -\tau_{\text{fb}} p + \frac{\partial a_1}{\partial \mu}\frac{u - u_w}{V_{\text{tip}}} + \frac{\partial a_1}{\partial \mu_z}\frac{w - w_w}{V_{\text{tip}}} + K_{\text{lon}} u_{\text{lon}} \tag{31}$$

where $\boldsymbol{w} = (u_w, v_w, w_w)^T$ is a vector of wind velocities. This avoids the need for state estimation of the flapping angles, which have no direct measurements. The approximated flapping then becomes part of the *algebraic* nonlinear equations of the main rotor-induced forces and moments.

Note that the coupled fuselage-rotor-stabilizer dynamics are described by second-order equations (lateral and longitudinal) with lightly damped resonance at relatively low frequencies due to the high time constant of the stabilizer bar flapping dynamics τ_{fb}, for example,

$$p(s) = \frac{L_\beta K_{\text{lat}}/\tau_{\text{fb}}}{s^2 + (1/\tau_{fb})s + L_\beta} u_{\text{lat}}$$

where $L_\beta = (h_{\text{mr}} T_{\text{mr}} + K_\beta)/I_{xx}$). These undesirable resonant modes can be corrected by means of simple notch filters to provide a critically damped second-order response

$$p(s) = \frac{L_\beta K_{\text{lat}}/\tau_{\text{fb}}}{s^2 + 2\sqrt{L_\beta} s + L_\beta} u_{\text{lat}}$$

and thus improve stability margins [28]. However, approximation of flapping in the steady state results in a first-order model

$$p(s) = \frac{L_\beta K_{\text{lat}}/\tau_{\text{fb}}}{(1/\tau_{fb})s + L_\beta} u_{\text{lat}}$$

that is too "optimistic" as it has higher bandwidth and larger stability margins than in reality and thus may cause attitude dynamics instability with a high-gain feedback control. This can be addressed either by appropriate choice of the SDRE cost matrices $\mathbf{Q}$ and $\mathbf{R}$ to limit the control bandwidth or by correcting the first-order model parameters in the SDRE formulation below, for example, decreasing K_{lat} and τ_{fb} by the same factor $k_1 > 1$ for a better approximation of the actual notched second-order lateral response

$$p(s) = \frac{L_\beta K_{\text{lat}}/\tau_{\text{fb}}}{(k_1/\tau_{fb})s + L_\beta} u_{\text{lat}}$$

A discussion of these ideas and illustrative Bode diagrams can be found in [28].

Assuming a small flapping magnitude due to the stiff rotor blade–hub assembly, the *approximate* expressions for the rotor forces and moments are given by

$$X_{\text{mr}} = -\left(-\tau_{\text{fb}} q + \frac{\partial a_1}{\partial \mu}\frac{u - u_w}{V_{\text{tip}}} + \frac{\partial a_1}{\partial \mu_z}\frac{w - w_w}{V_{\text{tip}}} + K_{\text{lon}} u_{\text{lon}}\right) T_{\text{mr}} \tag{32}$$

$$Y_{\text{mr}} = \left(-\tau_{\text{fb}} p + \frac{\partial b_1}{\partial \mu_v}\frac{v - v_w}{V_{\text{tip}}} + K_{\text{lat}} u_{\text{lat}}\right) T_{\text{mr}} \tag{33}$$

$$L_{\text{mr}} = \left(-\tau_{\text{fb}} p + \frac{\partial b_1}{\partial \mu_v}\frac{v - v_w}{V_{\text{tip}}} + K_{\text{lat}} u_{\text{lat}}\right)(h_{\text{mr}} T_{\text{mr}} + K_\beta) \tag{34}$$

$$M_{\text{mr}} = -\left(-\tau_{\text{fb}} q + \frac{\partial a_1}{\partial \mu}\frac{u - u_w}{V_{\text{tip}}} + \frac{\partial a_1}{\partial \mu_z}\frac{w - w_w}{V_{\text{tip}}} + K_{\text{lon}} u_{\text{lon}}\right)(h_{\text{mr}} T_{\text{mr}} + K_\beta) \tag{35}$$

To transform the dynamic Eqs. (5) into an SDC form, we first split the equations into three parts, i.e., rigid body dynamics without external forces and moments $\boldsymbol{f}_{\text{rb}}(\boldsymbol{x})$, accelerations due to external forces and moments that do not depend on control inputs $\boldsymbol{T}_d(\boldsymbol{x}, \boldsymbol{w})$, and rotor-induced accelerations $\boldsymbol{T}_u(\boldsymbol{x}, \boldsymbol{w})$:

$$\dot{\boldsymbol{x}} = \boldsymbol{f}_{\text{rb}}(\boldsymbol{x}) + \begin{pmatrix} \boldsymbol{T}_d(\boldsymbol{x}, \boldsymbol{w}) \\ 0 \end{pmatrix} + \begin{pmatrix} \boldsymbol{T}_u(\boldsymbol{x}, \boldsymbol{w}, \boldsymbol{u}) \\ 0 \end{pmatrix} \tag{36}$$

Explicitly,

$$\boldsymbol{f}_{\text{rb}}(\boldsymbol{x}) = \begin{pmatrix} -\boldsymbol{\Omega}\boldsymbol{v} \\ -\mathbf{I}^{-1}\boldsymbol{\Omega}\mathbf{I}\boldsymbol{\omega} \\ \boldsymbol{\Psi}(\boldsymbol{q})\boldsymbol{\omega} \\ \mathbf{R}(\boldsymbol{q})\boldsymbol{v} \end{pmatrix} \tag{37}$$

$$\boldsymbol{T}_d(\boldsymbol{x}, \boldsymbol{w}) = \begin{bmatrix} g\begin{pmatrix} -\sin\theta \\ \cos\theta\sin\phi \\ \cos\theta\cos\phi \end{pmatrix} + \frac{1}{m}(\boldsymbol{F}_{\text{fus}} + \boldsymbol{F}_{\text{vt}} + \boldsymbol{F}_{\text{ht}}) \\ \mathbf{I}^{-1}(\boldsymbol{M}_{\text{vt}} + \boldsymbol{M}_{\text{ht}}) \end{bmatrix} \tag{38}$$

$$\boldsymbol{T}_u(\boldsymbol{x}, \boldsymbol{w}, \boldsymbol{u}) = \begin{pmatrix} \frac{1}{m}(\boldsymbol{F}_{\text{mr}} + \boldsymbol{F}_{\text{tr}}) \\ \mathbf{I}^{-1}(\boldsymbol{M}_e + \boldsymbol{M}_{\text{mr}} + \boldsymbol{M}_{\text{tr}}) \end{pmatrix} \tag{39}$$

where $\boldsymbol{\Omega}$ is a cross-product matrix

$$\boldsymbol{\Omega} = \begin{pmatrix} 0 & -r & q \\ r & 0 & -p \\ -q & p & 0 \end{pmatrix}$$

The force-free rigid body dynamics $\boldsymbol{f}_{\text{rb}}(\boldsymbol{x})$ have an exact SDC parameterization:

$$\boldsymbol{f}_{\text{rb}}(\boldsymbol{x}) = \mathbf{A}_{\text{rb}}(\boldsymbol{x})\boldsymbol{x} \tag{40}$$

$$\mathbf{A}_{\text{rb}}(\boldsymbol{x}) = \begin{pmatrix} -\boldsymbol{\Omega} & \mathbf{0} & \mathbf{0} & \mathbf{0} \\ \mathbf{0} & -\mathbf{I}^{-1}\boldsymbol{\Omega}\mathbf{I} & \mathbf{0} & \mathbf{0} \\ \mathbf{0} & \boldsymbol{\Psi}(\boldsymbol{q}) & \mathbf{0} & \mathbf{0} \\ \mathbf{R}(\boldsymbol{q}) & \mathbf{0} & \mathbf{0} & \mathbf{0} \end{pmatrix} \tag{41}$$

Accelerations due to forces and moments from gravity, empennage, and fuselage drag (38) can be only approximately presented in an SDC form due to the gravity term $g\cos\theta\cos\phi$ not being zero in the origin $\boldsymbol{x} = \mathbf{0}$, downwash from rotors, and wind-induced drag and lift. Thus we further split $\boldsymbol{T}_d(\boldsymbol{x}, \boldsymbol{w})$ into two terms

$$\boldsymbol{T}_d(\boldsymbol{x}, \boldsymbol{w}) = \mathbf{A}_d(\boldsymbol{x}, \boldsymbol{w})\boldsymbol{x} + \Delta\boldsymbol{T}_d(\boldsymbol{x}, \boldsymbol{w}) \tag{42}$$

Note that the empennage and fuselage forces and moments are functions of vehicle velocities, wind, and implicitly (via rotors-induced downwash V_i) the collective control inputs u_{col}, u_{tcol}. The components due to the control inputs could be taken into account by linearizing $\boldsymbol{T}_d$; however, we chose to approximate it as independent of the control inputs and treated the downwash as a pseudoconstant, substituting its value in the expressions for the forces/moments with its past or trim value. Denoting SDC parameterization of forces (moments similarly) as $\boldsymbol{F} = \mathbf{F}^{\mathbf{v}}\boldsymbol{v} + \mathbf{F}^{\omega}\boldsymbol{\omega} + \Delta\boldsymbol{F}$, we have

$$\mathbf{A}_d(\boldsymbol{x}, \boldsymbol{w}) = \begin{pmatrix} \frac{1}{m}\left(\mathbf{F}^{\mathbf{v}}_{\text{fus}} + \mathbf{F}^{\mathbf{v}}_{\text{vt}} + \mathbf{F}^{\mathbf{v}}_{\text{ht}}\right) & \frac{1}{m}\left(\mathbf{F}^{\omega}_{\text{vt}} + \mathbf{F}^{\omega}_{\text{ht}}\right) & \mathbf{g}^{\mathbf{q}} & \mathbf{0} \\ \mathbf{I}^{-1}\left(\mathbf{M}^{\mathbf{v}}_{\text{vt}} + \mathbf{M}^{\mathbf{v}}_{\text{ht}}\right) & \mathbf{I}^{-1}\left(\mathbf{M}^{\omega}_{\text{vt}} + \mathbf{M}^{\omega}_{\text{ht}}\right) & \mathbf{0} & \mathbf{0} \end{pmatrix} \tag{43}$$

where the SDC form of acceleration due to gravity is given by

$$\mathbf{g}^{\mathbf{q}} = g\begin{pmatrix} 0 & -\frac{\sin\theta}{\theta} & 0 \\ \cos\theta\frac{\sin\phi}{\phi} & 0 & 0 \\ 0 & 0 & 0 \end{pmatrix}$$

and the parameterization of forces and moments is given by

$$\mathbf{F}^{\mathbf{v}}_{\text{fus}} + \mathbf{F}^{\mathbf{v}}_{\text{vt}} + \mathbf{F}^{\mathbf{v}}_{\text{ht}} = \begin{pmatrix} X^u_{\text{fus}} & 0 & 0 \\ 0 & Y^v_{\text{vt}} + Y^v_{\text{fus}} & \\ 0 & 0 & Z^w_{\text{ht}} + Z^w_{\text{fus}} \end{pmatrix}$$

$$\mathbf{F}^{\omega}_{\text{vt}} + \mathbf{F}^{\omega}_{\text{ht}} = \begin{pmatrix} 0 & 0 & 0 \\ 0 & 0 & Y^r_{\text{ct}} \\ 0 & Z^q_{\text{ht}} & 0 \end{pmatrix}$$

$$\mathbf{M}^{\mathbf{v}}_{\text{vt}} + \mathbf{M}^{\mathbf{v}}_{\text{ht}} = \begin{pmatrix} 0 & -z_{\text{vt}} Y^v_{\text{vt}} & 0 \\ 0 & 0 & -x_{\text{ht}} Z^w_{\text{ht}} \\ 0 & x_{\text{vt}} Y^v_{\text{vt}} & 0 \end{pmatrix}$$

$$\mathbf{M}^{\omega}_{\text{vt}} + \mathbf{M}^{\omega}_{\text{ht}} = \begin{pmatrix} 0 & 0 & -z_{\text{vt}} Y^r_{\text{vt}} \\ 0 & -x_{\text{ht}} Z^q_{\text{ht}} & 0 \\ 0 & 0 & x_{\text{vt}} Y^r_{\text{vt}} \end{pmatrix}$$

with known expressions for the forces and moments in the helicopter model,

$$X^u_{\text{fus}} = -0.5\rho S^{\text{fus}}_x V_\infty$$

$$Y^v_{\text{vt}} + Y^v_{\text{fus}} = 0.5\rho\Big[S_{\text{vt}}\Big(C^{\text{vt}}_{\text{La}} V^{\text{vt}}_\infty + |v_{\text{vt}}|\Big) - S^{\text{fus}}_y V_\infty\Big]$$

$$Z^w_{\text{ht}} + Z^w_{\text{fus}} = 0.5\rho\Big[S_{\text{ht}}\Big(C^{\text{ht}}_{\text{La}}|u - u_w| + |w_{\text{ht}}|\Big) - S^{\text{fus}}_z V_\infty\Big]$$

$$Y^r_{\text{vt}} = 0.5\rho S_{\text{vt}}\Big(C^{\text{vt}}_{\text{La}} V^{\text{vt}}_\infty + |v_{\text{vt}}|\Big) x_{\text{vt}}$$

$$Z^q_{\text{ht}} = -0.5\rho S_{\text{ht}}\Big(C^{\text{ht}}_{\text{La}}|u - u_w| + |w_{\text{ht}}|\Big) x_{\text{ht}}$$

The extra term $\Delta \boldsymbol{T}_d(\boldsymbol{x}, \boldsymbol{w})$ in (42) represents components of accelerations due to all remaining parts of forces and moments that could not be SDC parameterized. Although it is not necessary to explicitly calculate this term, it can be found if needed by simply writing $\Delta \boldsymbol{T}_d = \boldsymbol{T}_d - \mathbf{A}_d(\boldsymbol{x}, \boldsymbol{w})\boldsymbol{x}$.

Next consider the SDC parameterization of accelerations due to controls $\boldsymbol{T}_u$. Recall that extended linearization assumes the dynamics is linear in control. Equation (39) is defined in terms of the rotor-induced forces and moments and the engine torque. Rotor thrust is a nonlinear function of the helicopter and wind velocities and collective controls. Steady-state approximation of the flapping dynamics yields main rotor forces and moments (32–35) as bilinear functions of thrust and cyclic controls. To avoid linearization of the rotor thrust and computation of derivatives, we accept a new set of controls for the SDRE design, in which the collective control inputs are replaced with the main and tail rotor thrust: $\tilde{\boldsymbol{u}} = (u_{\text{lon}}, u_{\text{lat}}, T_{\text{mr}}, T_{\text{tr}})^T$. Thus, the SDC formulation changes to $\dot{\boldsymbol{x}} = \mathbf{A}(\boldsymbol{x})\boldsymbol{x} + \mathbf{B}(\boldsymbol{x})\tilde{\boldsymbol{u}}$. Note that the rotor thrust is a one-to-one mapping of the collective control input assuming steady and uniform inflow. The actual actuator inputs can be computed given a desired thrust numerically employing an iterative algorithm solving (13) and (14) with respect to u_{col} given the thrust coefficient C_T.

Next, we present the main rotor thrust as $T_{\text{mr}} = T^0_{\text{mr}} + \Delta T_{\text{mr}}$, where T^0_{mr} is either the trim value or the current thrust (the last control command) and ΔT_{mr} is an increment due to the new control command. Then from (39) and expressions of main rotor forces and moments (33–35), we have

$$\boldsymbol{T}_u(\boldsymbol{x}, \boldsymbol{w}, \boldsymbol{u}) \equiv \tilde{\boldsymbol{T}}_u(\boldsymbol{x}, \boldsymbol{w}, \tilde{\boldsymbol{u}}) = \mathbf{A}_u(\boldsymbol{x}, \boldsymbol{w})\boldsymbol{x} + \boldsymbol{G}_u(\boldsymbol{x}, \boldsymbol{w}, \tilde{\boldsymbol{u}})$$

where

$$\mathbf{A}_u(\boldsymbol{x}, \boldsymbol{w}) = \begin{pmatrix} \frac{1}{m}\mathbf{F}^{\mathbf{v}}_{\text{mr}} & \frac{1}{m}\mathbf{F}^{\omega}_{\text{mr}} & \mathbf{0} & \mathbf{0} \\ \mathbf{I}^{-1}\mathbf{M}^{\mathbf{v}}_{\text{mr}} & \mathbf{I}^{-1}\mathbf{M}^{\omega}_{\text{mr}} & \mathbf{0} & \mathbf{0} \end{pmatrix}$$

$$\boldsymbol{G}_u(\boldsymbol{x}, \boldsymbol{w}, \tilde{\boldsymbol{u}}) = \begin{pmatrix} \frac{1}{m}\boldsymbol{F}^{\tilde{\mathbf{u}}} \\ \mathbf{I}^{-1}\boldsymbol{M}^{\tilde{\mathbf{u}}} \end{pmatrix} \tag{44}$$

The elements of the block matrix $\mathbf{A}_u(\boldsymbol{x}, \boldsymbol{w})$ are

$$\mathbf{F}^{\mathbf{v}}_{\text{mr}} = \begin{pmatrix} X^u_{\text{mr}} & 0 & X^w_{\text{mr}} \\ 0 & Y^v_{\text{mr}} & 0 \\ 0 & 0 & 0 \end{pmatrix}, \qquad \mathbf{F}^{\omega}_{\text{mr}} = \begin{pmatrix} 0 & X^q_{\text{mr}} & 0 \\ Y^p_{\text{mr}} & 0 & 0 \\ 0 & 0 & 0 \end{pmatrix}$$

$$\mathbf{M}^{\mathbf{v}}_{\text{mr}} = \begin{pmatrix} 0 & L^v_{\text{mr}} & 0 \\ M^u_{\text{mr}} & 0 & M^w_{\text{mr}} \\ 0 & 0 & 0 \end{pmatrix}, \qquad \mathbf{M}^{\omega}_{\text{mr}} = \begin{pmatrix} L^p_{\text{mr}} & 0 & 0 \\ 0 & M^q_{\text{mr}} & 0 \\ 0 & 0 & 0 \end{pmatrix}$$

Their elements are easily derived from the rotor forces and moments Eqs. (33–35) as

$$X^u_{\text{mr}} = -\frac{T^0_{\text{mr}}}{V_{\text{tip}}}\frac{\partial a_1}{\partial \mu}, \qquad X^w_{\text{mr}} = -\frac{T^0_{\text{mr}}}{V_{\text{tip}}}\frac{\partial a_1}{\partial \mu_z}, \qquad X^q_{\text{mr}} = T^0_{\text{mr}}\tau_{\text{fb}}$$

$$Y^v_{\text{mr}} = \frac{T^0_{\text{mr}}}{V_{\text{tip}}}\frac{\partial b_1}{\partial \mu_v}, \qquad Y^p_{\text{mr}} = -T^0_{\text{mr}}\tau_{\text{fb}}$$

$$L^v_{\text{mr}} = (h_{\text{mr}}T^0_{\text{mr}} + K_\beta)\frac{1}{V_{\text{tip}}}\frac{\partial b_1}{\partial \mu_v}, \qquad L^p_{\text{mr}} = -(h_{\text{mr}}T^0_{\text{mr}} + K_\beta)\tau_{\text{fb}}$$

$$M^u_{\text{mr}} = -(h_{\text{mr}}T^0_{\text{mr}} + K_\beta)\frac{1}{V_{\text{tip}}}\frac{\partial a_1}{\partial \mu}$$

$$M^w_{\text{mr}} = -(h_{\text{mr}}T^0_{\text{mr}} + K_\beta)\frac{1}{V_{\text{tip}}}\frac{\partial a_1}{\partial \mu_z}, \qquad M^q_{\text{mr}} = (h_{\text{mr}}T^0_{\text{mr}} + K_\beta)\tau_{\text{fb}}$$

Elements of vector $\mathbf{G}_u(\boldsymbol{x}, \boldsymbol{w}, \tilde{\boldsymbol{u}})$ are then given by

$$\boldsymbol{F}^{\tilde{\boldsymbol{u}}} = \begin{pmatrix} -T^0_{\text{mr}}K_{\text{lon}}u_{\text{lon}} - \sin(a_1)\Delta T_{\text{mr}} \\ T^0_{\text{mr}}K_{\text{lat}}u_{\text{lat}} + \sin(b_1)\Delta T_{\text{mr}} - T_{\text{tr}} \\ -T_{\text{mr}} \end{pmatrix}$$

$$\boldsymbol{M}^{\tilde{\boldsymbol{u}}} = \begin{pmatrix} (h_{\text{mr}}T^0_{\text{mr}} + K_\beta)K_{\text{lat}}u_{\text{lat}} + \sin(b_1)h_{\text{mr}}\Delta T_{\text{mr}} + z_{\text{tr}}T_{\text{tr}} \\ (h_{\text{mr}}T^0_{\text{mr}} + K_\beta)K_{\text{lon}}u_{\text{lon}} + \sin(a_1)h_{\text{mr}}\Delta T_{\text{mr}} \\ -Q_e - x_{\text{tr}}T_{\text{tr}} \end{pmatrix}$$

Approximating engine torque with the main rotor aerodynamic torque (16) and assuming small flapping magnitude ($a_1 \approx 0, b_1 \approx 0$) using the fact that a hingeless rotor and stiff short rotor blades limit flapping to very low angles, we get

$$\boldsymbol{G}_u(\boldsymbol{x}, \boldsymbol{w}, \tilde{\boldsymbol{u}}) = \mathbf{B}_u(\boldsymbol{x}, \boldsymbol{w})\tilde{\boldsymbol{u}} + \Delta\tilde{\boldsymbol{T}}_u(\boldsymbol{x}, \boldsymbol{w}, \tilde{\boldsymbol{u}})$$

where in case of a diagonal inertia matrix

$$\mathbf{B}_u(\boldsymbol{x}, \boldsymbol{w}) = \begin{pmatrix} -\frac{T^0_{\text{mr}}K_{\text{lon}}}{m} & 0 & 0 & 0 \\ 0 & \frac{T^0_{\text{mr}}K_{\text{lat}}}{m} & 0 & -\frac{1}{m} \\ 0 & 0 & -\frac{1}{m} & 0 \\ 0 & \frac{(h_{\text{mr}}T^0_{\text{mr}} + K_\beta)K_{\text{lat}}}{I_{xx}} & 0 & \frac{z_{\text{tr}}}{I_{xx}} \\ \frac{(h_{\text{mr}}T^0_{\text{mr}} + K_\beta)K_{\text{lon}}}{I_{yy}} & 0 & 0 & 0 \\ 0 & 0 & -\frac{R_{\text{mr}}(\lambda_0 - \mu_z)}{I_{zz}} & -\frac{x_{\text{tr}}}{I_{zz}} \end{pmatrix}$$

and the extra term $\Delta\tilde{\boldsymbol{T}}_u(\boldsymbol{x}, \boldsymbol{w}, \tilde{\boldsymbol{u}})$ contains accelerations due to neglected bilinearities and the engine torque approximation. Again, it can be computed if necessary as $\Delta\tilde{\boldsymbol{T}}_u = \tilde{\boldsymbol{T}}_u - \mathbf{A}_u(\boldsymbol{x}, \boldsymbol{w})\boldsymbol{x} - \mathbf{B}_u(\boldsymbol{x}, \boldsymbol{w})\tilde{\boldsymbol{u}}$. Thus, the SDC parameterization of (39) is given by

$$\boldsymbol{T}_u(\boldsymbol{x}, \boldsymbol{w}, \boldsymbol{u}) \equiv \tilde{\boldsymbol{T}}_u(\boldsymbol{x}, \boldsymbol{w}, \tilde{\boldsymbol{u}}) = \mathbf{A}_u(\boldsymbol{x}, \boldsymbol{w})\boldsymbol{x} + \mathbf{B}_u(\boldsymbol{x}, \boldsymbol{w})\tilde{\boldsymbol{u}} + \Delta\tilde{\boldsymbol{T}}_u(\boldsymbol{x}, \boldsymbol{w}, \tilde{\boldsymbol{u}}) \tag{45}$$

Note that although the bilinear control terms (e.g., $\sin(a_1)\Delta T_{\text{mr}}$ and $\sin(b_1)\Delta T_{\text{mr}}$) have to be discarded from consideration, this does not introduce significant approximation errors due to the dominant influence of the stiff hingeless rotor blade–hub assembly (large K_β). Alternatively, the bilinearity due to approximated flapping can further be eliminated by presenting the control inputs as part of a new state space $\boldsymbol{x}^* = (\boldsymbol{x}, \tilde{\boldsymbol{u}})$ and introducing new "controls" $\dot{\tilde{\boldsymbol{u}}} = \boldsymbol{u}^*$. Such an approach, however, would increase the model order, and limited onboard computational resources may prohibit its use.

Finally, to construct the system matrices $\mathbf{A}(\boldsymbol{x})$ and $\mathbf{B}(\boldsymbol{x})$, Eqs. (40), (42), and (45) are gathered together yielding

$$\mathbf{A}(\boldsymbol{x},\boldsymbol{w}) = \mathbf{A}_{\text{rb}}(\boldsymbol{x}) + \begin{pmatrix} \mathbf{A}_d(\boldsymbol{x},\boldsymbol{w}) \\ \mathbf{0}^{6\times 12} \end{pmatrix} + \begin{pmatrix} \mathbf{A}_u(\boldsymbol{x},\boldsymbol{w}) \\ \mathbf{0}^{6\times 12} \end{pmatrix}$$
$$\mathbf{B}(\boldsymbol{x},\boldsymbol{w}) = \begin{pmatrix} \mathbf{B}_u(\boldsymbol{x},\boldsymbol{w}) \\ \mathbf{0}^{6\times 4} \end{pmatrix} \tag{46}$$

$$\Delta \boldsymbol{f}(\boldsymbol{x},\boldsymbol{w},\boldsymbol{u}) = \begin{pmatrix} \Delta \boldsymbol{T}_d(\boldsymbol{x},\boldsymbol{w}) \\ \mathbf{0} \end{pmatrix} + \begin{pmatrix} \Delta \tilde{\boldsymbol{T}}_u(\boldsymbol{x},\boldsymbol{w},\tilde{\boldsymbol{u}}) \\ \mathbf{0} \end{pmatrix} \tag{47}$$

One can observe that the obtained $\mathbf{A}(\boldsymbol{x},\boldsymbol{w})$ and $\mathbf{B}(\boldsymbol{x},\boldsymbol{w})$ are bounded and continuous almost everywhere on a compact set of $\boldsymbol{x}$. (The condition does not hold, however, at pitch angles of ± 90 deg due to use of Euler angles in the matrix $\boldsymbol{\Psi}(\boldsymbol{q})$. To avoid this, we assigned a 5 deg "dead zone" around the critical pitch angles so that they are not used in the computation of $\mathbf{A}(\boldsymbol{x})$ and $\mathbf{B}(\boldsymbol{x})$. Another solution would be using quaternions instead of Euler angles in the SDRE formulation.) Discrete system matrices $\boldsymbol{\Phi}(\boldsymbol{x}_k,\boldsymbol{w}_k)$ and $\Gamma(\boldsymbol{x}_k,\boldsymbol{w}_k)$ are obtained from $\mathbf{A}(\boldsymbol{x},\boldsymbol{w})$ and $\mathbf{B}(\boldsymbol{x},\boldsymbol{w})$ by approximate discretization at each time step, i.e., $\boldsymbol{\Phi}(\boldsymbol{x}_k,\boldsymbol{w}_k) \approx e^{\mathbf{A}(\boldsymbol{x}_k,\boldsymbol{w}_k)\Delta t}$, $\Gamma(\boldsymbol{x}_k,\boldsymbol{w}_k) \approx \mathbf{B}(\boldsymbol{x}_k,\boldsymbol{w}_k)\Delta t$.

Compensator Design

The compensator is designed to cancel the mismatch $\Delta \boldsymbol{f}(\boldsymbol{x},\boldsymbol{w},\tilde{\boldsymbol{u}})$ between the original dynamics and its SDC parameterization and provide the reference input, or trim control. To do this, the control is computed as a sum of the SDRE output and the compensator correction, $\boldsymbol{u} = \boldsymbol{u}^{\text{sd}} + \boldsymbol{u}^c$, such that the following holds: $\dot{\boldsymbol{e}} = \mathbf{A}(\boldsymbol{x},\boldsymbol{w})\boldsymbol{e} + \mathbf{B}(\boldsymbol{x})\tilde{\boldsymbol{u}}^{\text{sd}}$. This implies,

$$\boldsymbol{f}_{\text{rb}}(\boldsymbol{x}) + \begin{pmatrix} \boldsymbol{T}_d(\boldsymbol{x},\boldsymbol{w}) \\ \mathbf{0} \end{pmatrix} + \begin{pmatrix} \boldsymbol{T}_u(\boldsymbol{x},\boldsymbol{w},\boldsymbol{u}^{\text{sd}}+\boldsymbol{u}^c) \\ \mathbf{0} \end{pmatrix} - \dot{\boldsymbol{x}}_{\text{des}} = \mathbf{A}(\boldsymbol{x},\boldsymbol{w})\boldsymbol{e} + \mathbf{B}(\boldsymbol{x},\boldsymbol{w})\tilde{\boldsymbol{u}}^{\text{sd}} \tag{48}$$

Note that $\boldsymbol{u}^{\text{sd}} = (u_{\text{lon}}, u_{\text{lat}}, u_{\text{col}}, u_{\text{tcol}})^T$ and $\tilde{\boldsymbol{u}}^{\text{sd}} = (u_{\text{lon}}, u_{\text{lat}}, T_{\text{mr}}, T_{\text{tr}})^T$, as discussed in the previous section. Let $\dot{\boldsymbol{q}}_{\text{des}} = \boldsymbol{\Psi}(\boldsymbol{q})\boldsymbol{\omega}_{\text{des}}$ and $\dot{\boldsymbol{p}}_{\text{des}} = \mathbf{R}(\boldsymbol{q})\boldsymbol{v}_{\text{des}}$, and for convenience define the vector $\boldsymbol{D}(\boldsymbol{x},\boldsymbol{w},\tilde{\boldsymbol{u}}^{\text{sd}})$ as

$$\boldsymbol{D} = -\boldsymbol{f}_{\text{rb}}^{\mathbf{v},\omega} + \begin{pmatrix} \dot{\boldsymbol{v}}_{\text{des}} \\ \dot{\boldsymbol{\omega}}_{\text{des}} \end{pmatrix} + \mathbf{A}^{\mathbf{v},\omega}(\boldsymbol{x},\boldsymbol{w})\boldsymbol{e} + \mathbf{B}_u(\boldsymbol{x},\boldsymbol{w})\tilde{\boldsymbol{u}}^{\text{sd}} - \boldsymbol{T}_d(\boldsymbol{x},\boldsymbol{w}) \tag{49}$$

where $\boldsymbol{f}_{\text{rb}}^{\mathbf{v},\omega}$ and $\mathbf{A}^{\mathbf{v},\omega}(\boldsymbol{x},\boldsymbol{w})$ are upper halves of (37) and (46),

$$\boldsymbol{f}_{\text{rb}}^{\mathbf{v},\omega}(\boldsymbol{x}) = \begin{pmatrix} -\boldsymbol{\Omega}\boldsymbol{v} \\ -\mathbf{I}^{-1}\boldsymbol{\Omega}\mathbf{I}\boldsymbol{\omega} \end{pmatrix}$$
$$\mathbf{A}^{\mathbf{v},\omega}(\boldsymbol{x},\boldsymbol{w}) = \begin{pmatrix} -\boldsymbol{\Omega} & \mathbf{0} & \mathbf{0} & \mathbf{0} \\ \mathbf{0} & -\mathbf{I}^{-1}\boldsymbol{\Omega}\mathbf{I} & \mathbf{0} & \mathbf{0} \end{pmatrix} + \mathbf{A}_d(\boldsymbol{x},\boldsymbol{w}) + \mathbf{A}_u(\boldsymbol{x},\boldsymbol{w})$$

Then (48) can be rewritten as

$$\boldsymbol{T}_u(\boldsymbol{x},\boldsymbol{w},\boldsymbol{u}^{\text{sd}}+\boldsymbol{u}^c) = \boldsymbol{D}(\boldsymbol{x},\boldsymbol{w},\tilde{\boldsymbol{u}}^{\text{sd}}) \tag{50}$$

If the operator $\boldsymbol{T}_u(\boldsymbol{x},\boldsymbol{w},\boldsymbol{u})$ was control invertible, the compensator output could then be computed as $\boldsymbol{u}^c = \boldsymbol{T}_u^{-1}(\boldsymbol{x},\boldsymbol{w},\boldsymbol{D}(\boldsymbol{x},\boldsymbol{w},\tilde{\boldsymbol{u}}^{\text{sd}})) - \boldsymbol{u}^{\text{sd}}$. Unfortunately, a helicopter is an underactuated system, and $\boldsymbol{T}_u$ establishes a mapping from $U \subset R^4$ (4 control inputs) to a four-dimensional manifold in R^6. Thus equality in (48) or (50) may be attained only when values of $\boldsymbol{D}$ happen to be on the same manifold, which generally is not the case. Thus, $\boldsymbol{T}_u(\boldsymbol{x},\boldsymbol{w},\boldsymbol{u})$ is not control invertible, and an approximate solution must be found. To do this, we note that the translational motion of a helicopter in the x–y plane is dominated by the vehicle attitude rather than by the direct effect of the main rotor disk tilting due to flapping. Thus we can neglect direct coupling between the translational dynamics and cyclic control inputs in the compensator design (assuming small flapping magnitude a_1 and b_1). Such an assumption is also reinforced by the specific helicopter construction that limits flapping magnitude: hingeless rotor hub and relatively short stiff rotor blades. Discarding from consideration the translational dynamics (elements T_1, T_2, D_1 and D_2), we obtain the new truncated operators $\boldsymbol{D}^*(\boldsymbol{x},\boldsymbol{w},\tilde{\boldsymbol{u}}^{\text{sd}}) = \{D_i\}_{i=3}^6$ and

$$\boldsymbol{T}_u^*(\boldsymbol{x},\boldsymbol{w},\boldsymbol{u}) = \{T_i\}_{i=3}^6 \equiv \begin{pmatrix} \frac{1}{m} Z_{\text{mr}} \\ \mathbf{I}^{-1}(\boldsymbol{M}_e + \boldsymbol{M}_{\text{mr}} + \boldsymbol{M}_{\text{tr}}) \end{pmatrix}$$

Explicitly,

$$\boldsymbol{T}_u^* = \begin{pmatrix} -\frac{1}{m} T_{\text{mr}} \\ \frac{1}{I_{xx}}(h_{\text{mr}} T_{\text{mr}} + K_\beta)\sin(b_1) + z_{\text{tr}} T_{\text{tr}} \\ \frac{1}{I_{yy}}(h_{\text{mr}} T_{\text{mr}} + K_\beta)\sin(a_1) + Q_{\text{tr}} \\ \frac{1}{I_{zz}}(-x_{\text{tr}} T_{\text{tr}} - Q_e) \end{pmatrix} \tag{51}$$

omitting dependence on $\boldsymbol{x}$ and $\boldsymbol{w}$ for brevity and assuming a diagonal inertia matrix.

The new operator $\boldsymbol{T}_u^*(\boldsymbol{x},\boldsymbol{w},\boldsymbol{u})$ is control invertible, and thus the compensator output is given by $\boldsymbol{u}^c = \boldsymbol{T}_u^{*^{-1}}(\boldsymbol{x},\boldsymbol{w},\boldsymbol{D}^*(\boldsymbol{x},\boldsymbol{w},\tilde{\boldsymbol{u}}^{\text{sd}})) - \boldsymbol{u}^{\text{sd}}$. The proof is based on the inverse function theorem, which can be found in most texts on advanced calculus [29]. It suffices to show that $\partial \boldsymbol{T}_u^*(\boldsymbol{x},\boldsymbol{w},\boldsymbol{u})/\partial \boldsymbol{u}$ is nonsingular everywhere the compensator output is computed. Using a small angle approximation, direct computation of the Jacobian yields

$$\frac{\partial \boldsymbol{T}_u^*}{\partial \boldsymbol{u}} = \begin{pmatrix} 0 & 0 & -\frac{1}{m}\frac{\partial T_{\text{mr}}}{\partial u_{\text{col}}} & 0 \\ 0 & \frac{(h_{\text{mr}} T_{\text{mr}} + K_\beta) K_{\text{lat}}}{I_{xx}} & \frac{b_1 h_{\text{mr}}}{I_{xx}}\frac{\partial T_{\text{mr}}}{\partial u_{\text{col}}} & \frac{z_{\text{tr}}}{I_{xx}}\frac{\partial T_{\text{tr}}}{\partial u_{\text{tcol}}} \\ \frac{(h_{\text{mr}} T_{\text{mr}} + K_\beta) K_{\text{lon}}}{I_{yy}} & 0 & \frac{a_1 h_{\text{mr}}}{I_{yy}}\frac{\partial T_{\text{mr}}}{\partial u_{\text{col}}} & \frac{1}{I_{yy}}\frac{\partial Q_{\text{tr}}}{\partial u_{\text{tcol}}} \\ 0 & 0 & -\frac{1}{I_{zz}}\frac{\partial Q_e}{\partial u_{\text{col}}} & -\frac{x_{\text{tr}}}{I_{zz}}\frac{\partial T_{\text{tr}}}{\partial u_{\text{tcol}}} \end{pmatrix}$$

This Jacobian is nonsingular everywhere in the state and control space except the subset of $X \times W \times U$, where $\partial T_{\text{mr}}(\boldsymbol{x},\boldsymbol{w},u_{\text{col}})/\partial u_{\text{col}} = 0$ or $\partial T_{\text{tr}}(\boldsymbol{x},\boldsymbol{w},u_{\text{tcol}})/\partial u_{\text{tcol}} = 0$, which is of no interest for us because this is where the system becomes uncontrollable (e.g., vortex ring condition [27]). Therefore, $\boldsymbol{T}_u^*$ is control invertible, and the compensator output can be computed as stated.

Although $\boldsymbol{T}_u^*(\boldsymbol{x},\boldsymbol{w},\boldsymbol{u})$ is a nonlinear operator, its inverse is easy to compute due to the fact that forces and moments factor with respect to the control inputs. This allows us to compute $\boldsymbol{T}_u^{*^{-1}}(\boldsymbol{x},\boldsymbol{w},\boldsymbol{D}^*)$ by computing its four elements sequentially. Because $\boldsymbol{u} = \boldsymbol{u}^{\text{sd}} + \boldsymbol{u}^c$, from (51) we have

$$u_{\text{col}}^c = T_{\text{mr}}^{-1}(\boldsymbol{x},\boldsymbol{w},mD_3) - u_{\text{col}}^{\text{sd}}$$
$$u_{\text{tcol}}^c = T_{\text{tr}}^{-1}\left(\boldsymbol{x},\boldsymbol{w},\frac{I_{zz}D_6 + Q_e\left(u_{\text{col}}^{\text{sd}} + u_{\text{col}}^c\right)}{x_{\text{tr}}}\right) - u_{\text{tcol}}^{\text{sd}}$$
$$u_{\text{lat}}^c = \left[\arcsin\left(\frac{I_{xx}D_4 - z_{\text{tr}}T_{\text{tr}}\left(u_{\text{tcol}}^{\text{sd}} + u_{\text{tcol}}^c\right)}{h_{\text{mr}}T_{\text{mr}}\left(u_{\text{col}}^{\text{sd}} + u_{\text{col}}^c\right) + K_\beta}\right) + \tau_{\text{fb}}p - \frac{\partial b_1}{\partial \mu_v}\frac{v_a}{V_{\text{tip}}}\right]\frac{1}{K_{\text{lat}}} - u_{\text{lat}}^{\text{sd}}$$
$$u_{\text{lon}}^c = \left[\arcsin\left(\frac{I_{yy}D_5 - Q_{\text{tr}}\left(u_{\text{tcol}}^{\text{sd}} + u_{\text{tcol}}^c\right)}{h_{\text{mr}}T_{\text{mr}}(u_{\text{col}}^{\text{sd}} + u_{\text{col}}^c) + K_\beta}\right) + \tau_{\text{fb}}q - \frac{\partial a_1}{\partial \mu}\frac{u_a}{V_{\text{tip}}} - \frac{\partial a_1}{\partial \mu_z}\frac{w_a}{V_{\text{tip}}}\right]\frac{1}{K_{\text{lon}}} - u_{\text{lon}}^{\text{sd}}$$

where the rotor thrust inverses T_{mr}^{-1} and T_{tr}^{-1} are computed numerically employing an iterative algorithm solving (13) and (14) with respect to u_{col} given the thrust coefficient C_T.

In the following section we demonstrate experimental results and highlight the difference due to the SDRE augmentation with the designed compensator.

Experimental Results

Software Simulations

The simulation environment for the XCell-90 helicopter is derived from a software package developed at MIT's Information Control Engineering program for the Aerial Robotics Project. Results presented in this section were obtained with a Matlab implementation of the simulator that used the full software model developed by MIT in the form of a compiled Matlab mex-function. Additionally, a 10 ms control delay is simulated to account for state estimation and control computation time in real flight. Simulation results and description of the GTMAX software model are omitted for the sake of brevity. The XCell-90 simulation vehicle model [19] includes a generic small helicopter model described in previous sections with four actuators modeled as third-order linear systems and a PI engine governor. The avionics box is modeled as being flexibly connected to the vehicle frame. Sensors (GPS, IMU, barometric altimeter, and compass) are modeled to have biases, noise, latencies, and phase delays. Additionally, the IMU has low-pass filters on its outputs. The altimeter output is quantized. Loss of the GPS reception and reacquisition delay are simulated when the fuselage is tilted to more than 78 deg from the Earth vertical. A standard extended Kalman filter (EKF) is used for state estimation.

Experiment 1: Compensator vs Fixed Trim

We compared the augmented SDRE design versus an SDRE with a simple fixed trim control. The test trajectory used in the experiment consists of a takeoff and rapid ascent at 5 m/s, acceleration to 15 m/s forward flight, diving into a "figure-8" maneuver at 5 m/s descent speed with an immediate ascent during the second half of the maneuver at 5 m/s ascent speed, followed by a straight path, and finally a rapid deceleration to 2 m/s (see Fig. 4). To illustrate the performance difference, the yaw is also shown. One can easily associate spikes in heading with the onset of specific maneuvers for the SDRE with trim control: takeoff and climb, 0–18 s; hover, 18–23 s; acceleration and level flight, 23–33 s; diving into the left turn, 33–43 s; ascending into the right turn, 43–53 s; level flight, 53–58 s; and deceleration and level flight, 58–68 s. The improved performance provided by the compensator is clearly seen.

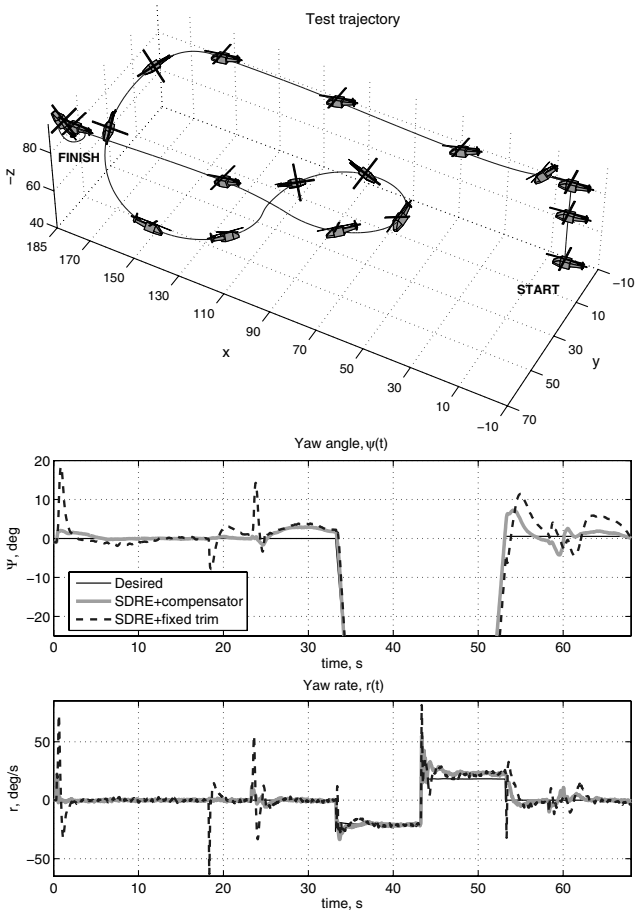

Fig. 4 SDRE + compensator vs SDRE + fixed trim control.

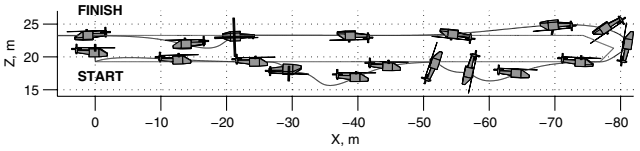

Fig. 5 Trajectory with rolls and inverted flight.

Experiment 2: Rolls, Loops, and Inverted Flight

To demonstrate agile maneuvering capabilities, we simulated a trajectory (see Fig. 5) consisting of 1) a vertical climb at 5 m/s; 2) forward flight at 5 m/s; 3) a 360 deg roll (around the x body axis) performed by commanding a 180 deg/s roll rate; 4) forward flight; 5) a 360 deg backward "tumble" (around the y body axis) performed by commanding constant forward velocity in the inertial frame and a 180 deg/s pitch rate at a constant altitude; 6) forward flight; 7) a U-turn by executing a half-loop at a 180 deg/s pitch rate into inverted flight with a 3 m altitude gain and accelerating forward to commanded 5 m/s speed; 8) forward inverted flight; and 9) a half-roll into normal forward flight towards the starting point. The trajectory was simulated using the true state information (the EKF position estimate drifts away due to the GPS outage during inverted flight). The entire trajectory is controlled by a common closed-loop controller without mode switching to separate control logic. Thus it illustrates the capability of an augmented SDRE autopilot to provide modeless control throughout a series of maneuvers. The top and middle plots in Fig. 6 show the roll and pitch response during execution of the trajectory. Attitude response closely follows the desired trajectory (note that the range of pitch is from −90 to 90 deg; thus, the roll and yaw angles flip 180 deg when the pitch reaches its extreme values). One can also notice a slight lag in the attitude response (zoomed in upon in Fig. 7). This lag is due to the presence of the stabilizer bar and its high time constant τ_{fb} in the flapping dynamics (6) and (7) (recall that, for the XCell-90, $\tau_{\text{fb}} = 0.12$ s).

Execution of rolls and loops demands cyclic controls at nearly saturation levels, and the lag due to the flapping time constant is practically unavoidable. The bottom plot of Fig. 6 demonstrates vehicle altitude throughout the trajectory. We had to reduce position (and side–forward velocity) tracking during execution of rolls and loops to minimize the altitude loss by avoiding conflicts when the altitude error and its rate reduce or even reverse cyclic control commands through weighting action of the SDRE gain matrix. Altitude loss during rolls and loops can be further decreased by modifying the desired trajectory to include a short burst of the main rotor thrust to gain extra lift just before execution of rolls as human pilots do.

Experiment 3: Wind Disturbance Mitigation

The next set of plots (Fig. 8) demonstrates the potential improvement in control accuracy when a constant wind disturbance is mitigated by taking the wind into account in the augmented SDRE design. The desired trajectory consists of several segments: a vertical climb to hover, followed by a square at 5 m/s, then a forward circle at 10 m/s, and a second circle with the nose pointed to the center flown at 10 m/s. Simulation plots show three cases: flight in still air, flight with a 5 m/s unaccounted for South-East wind, and the same flight when the wind velocity estimate is used in the control design. When a constant wind is added to the simulated environment but is not

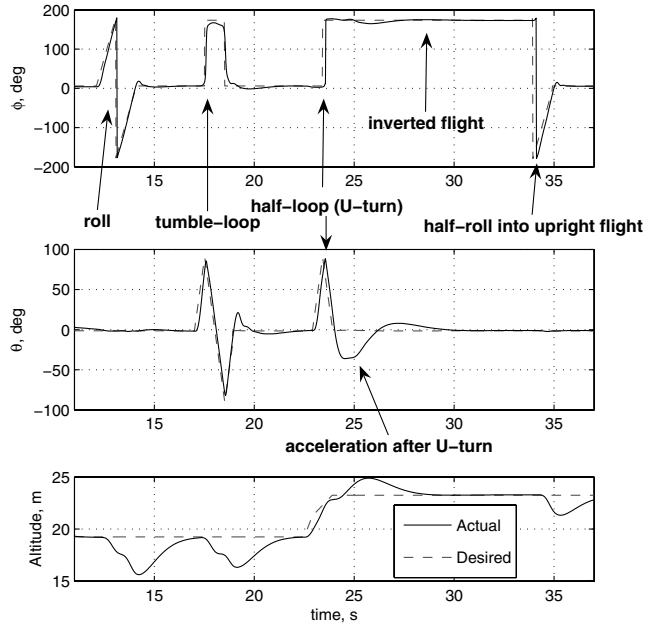

Fig. 6 Roll (top) and pitch (middle) response and altitude tracking (bottom).

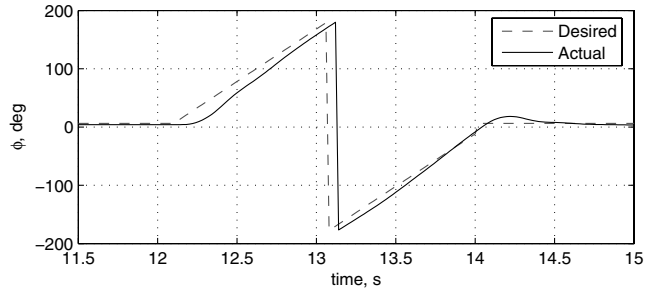

Fig. 7 Lag in the roll response due to the stabilizer bar.

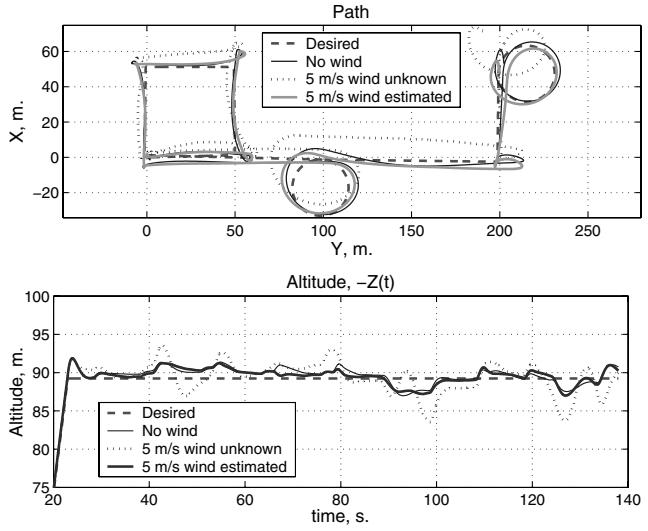

Fig. 8 Wind disturbance mitigation.

compensated for in the controller, tracking quality diminishes. This is a direct result of unaccounted for wind-induced terms in the SDC formulation, which become more dominant as the wind increases. Poorer altitude hold is especially noticeable in mode transitions where attitude changes result in abrupt wind airflow patterns relative to the main rotor disk thus creating rapid fluctuations in the rotor thrust. Given a wind estimate, the designed control is able to provide nearly the same accuracy in tracking as if there were no wind (see the bold solid plots in Fig. 8). If an estimate of the wind velocities is not available, simple integral control on positions can also be used to improve trajectory tracking.

Table 2 Variation of model parameters from nominal values for robustness evaluation

Parameter	Range of values
Principal moments of inertia, I_{xx}, I_{yy}, and I_{zz}	±20%
Cross-axis moment of inertia, I_{xz}	−0.03–0.03 kg · m^2
Variation of mass due to fuel consumption in flight	±5%
Main and tail rotor lift curve slope	±20%
Main and tail rotor profile drag coefficients	±20%
Longitudinal and lateral cyclic-to-flap gains, K_{lon} and K_{lat}	±20%
Engine governor gain	±50%
Flap response to speed gain, K_μ	±50%
Main rotor hub torsional stiffness, K_β	±10%
Fuselage areas	±50%

Experiment 4: Robustness to Model Parameters, State Estimation, and Latency

Of practical importance to any control design is the ability to provide acceptable performance when state measurements are not accurate or model parameters differ from the nominal parameters used in the design. The robustness to model parameters variation is usually provided either through direct accounting for a certain range of the parameters, such that the designed control will perform satisfactorily for any set of parameters in range (e.g., LPV, H_∞ control), or by means of adaptive control. Because model parameter ranges were not accounted for in the design of the autopilot, in this section we simply test control performance with different parameter combinations to evaluate its robustness. Ranges and variation of the model parameters from the nominal values are shown in Table 2. The worst case parameters were grouped together to constitute two experiments in addition to the case with nominal values: Group 1 consists of high mass, high moments of inertia, and low gains; group 2 consists of low mass, low moments of inertia, and high gains.

A test trajectory was designed that includes different flight modes and larger rotor thrust variations. The trajectory consists of lift, hover, acceleration into a backward flight at 8 m/s speed, a repeated sequence of an upward (3 m/s) clockwise spiral (as viewed from above) followed by a counter-clockwise downward spiral, and deceleration into hover (Fig. 9). In the backward flight, vertical and horizontal tails work as antistabilizers, and thus the difference in control performance is more pronounced when model parameters or state estimates are inaccurate.

To evaluate robustness to the inaccurate state estimation, we used a standard EKF, the parameters of which were set to provide slowly converging estimates of IMU biases. This resulted in a yaw estimation bias error slowly decreasing from 7 to 2 deg and mean velocity errors of 0.5 m/s, with a maximum of 1.3 m/s throughout the simulated flight.

The simulation results are presented in Table 3. The table displays mean state error costs and root mean square (RMS) errors as a measure of robustness to parameter variation and state estimation. Specifically, we simulated the case of nominal parameters using both accurate state information and the EKF estimates and the two parameter groups described above using the EKF. The case of nominal parameters with accurate state measurements vs the EKF is additionally illustrated in Fig. 10. The results demonstrate better tracking performance of the SDRE compared with the LQR (both the SDRE and the LQR were tested in combination with the compensator). One can see that most of the performance degradation is due to imperfect state estimation, which is a significant limiting factor even when model parameters are known precisely. The performance degrades nearly by a factor of 4, RMS position error is increased about 2.5 times, RMS velocity error is 1.76 times larger, and RMS attitude error grows more than 1.5 times. Thus, more

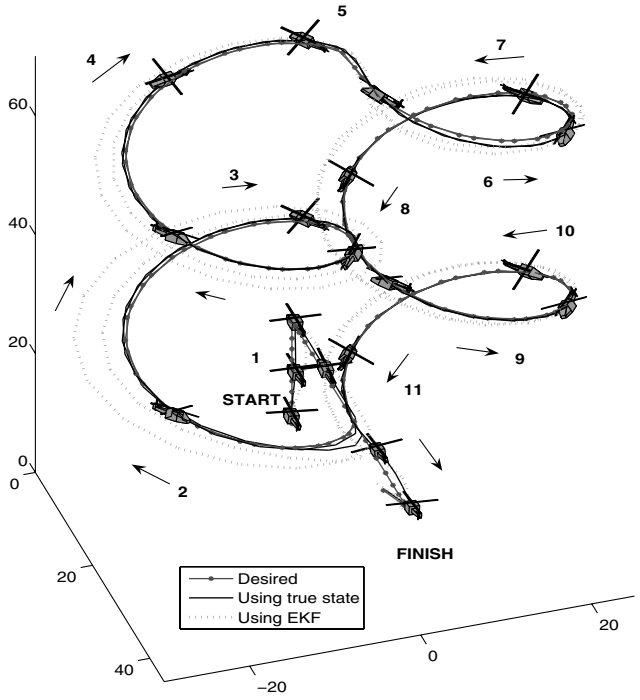

Fig. 9 Test trajectory for robustness evaluation.

accurate state estimation techniques may present relatively high-performance gains [30]. Another observation from the test results is that the SDRE appears to have more *relative* sensitivity to parameter variations than the LQR, i.e., the SDRE performance improvement over LQR is less with inaccurate parameters than in the case of the exact known model parameters. The SDRE tends to be more conservative. Improvement in position errors over the LQR decreases, but the relative difference in attitude and angular rates tracking becomes more pronounced. To stress the difference during the robustness evaluation, we increased weights on position tracking in matrix **Q**. We observed that on less aggressive trajectories with lower control gains the SDRE did not demonstrate as much of an improvement. This observation is in accordance with the fact that the SDRE behaves similarly to the LQR near equilibrium (system

Table 3 Robustness evaluation results.

	LQR	SDRE	Improvement, %
Nominal + True state			
Full state cost	**5.67**	**4.23**	25.4
RMS position error, m	1.17	0.89	23.8
RMS velocity error, m/s	1.02	0.82	20.2
RMS attitude error, deg	4.01	3.61	10.0
RMS rates (p, q, r) error, deg /s	8.82	8.54	3.2
Nominal + EKF			
Full state cost	**22.47**	**16.51**	26.5
RMS position error, m	2.91	2.46	15.6
RMS velocity error, m/s	1.87	1.49	19.9
RMS attitude error, deg	6.47	5.61	13.3
RMS rates (p, q, r) error, deg /s	11.34	10.54	7.1
Group 1 + EKF			
Full state cost	**25.51**	**22.01**	13.6
RMS position error, m	3.13	2.93	6.6
RMS velocity error, m/s	1.93	1.67	13.8
RMS attitude error, deg	7.39	6.25	15.5
RMS rates (p, q, r) error, deg /s	11.97	11.12	7.2
Group 2 + EKF			
Full state cost	**24.04**	**19.31**	19.7
RMS position error, m	2.98	2.68	10.1
RMS velocity error, m/s	1.83	1.54	15.9
RMS attitude error, deg	7.68	6.53	14.9
RMS rates (p, q, r) error, deg /s	12.38	11.23	9.3

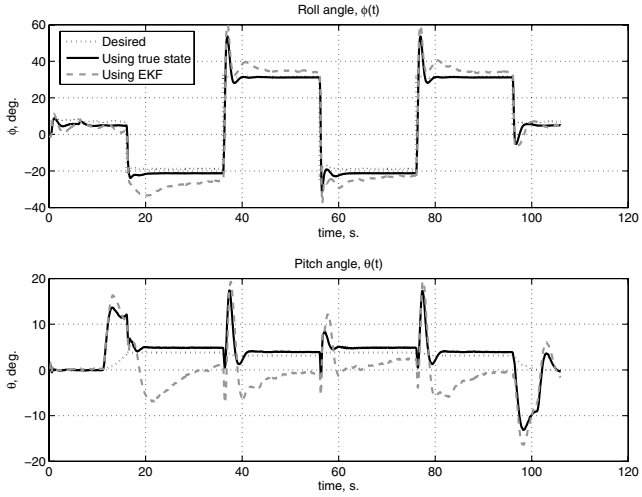

Fig. 10 SDRE performance using true state information vs the EKF.

equations in the SDC form approximate linearized equations used in the LQR design at the origin [4,17]).

We next tested robustness of the designed control law at nominal model parameters to latencies in the control loop (recall that the Yamaha control system has a 180 ms latency in transmitting commands to the actuators). For the latency test, we used a simpler trajectory consisting of a figure 8 flown backwards. Ideally, latency should be compensated by taking it into account in the control design. In the case of continuous control design, a Pade approximation can be used to approximate pure time delay with a dynamic phase shift. In the discrete case, if the latency can be expressed as a multiple of sampling intervals, simple extension of the state vector explicitly includes latency into the model. The major drawback of such a simple approach is that the order of the model grows proportionally to the latency. In our case, the model order of the system with the 10 sample delay would be 52, which would make it unacceptable for onboard application. A computationally "cheap" alternative that we used was to increase the phase margin by adjusting state and control cost matrices **Q** and **R**, which results in lower control gains. For the latency tests, we performed a number of simulations: nominal control design (nominal **Q** and **R**), lower control gains (for simplicity, we kept **R** the same and adjusted **Q**), and latency included in the control design via the state vector extension. Additionally we simulated a case with nominal parameters and "decoupled" main and tail rotor controls by specifying yaw dynamics as independent of the main rotor torque. In this case, the compensator adjusts the tail rotor control input to counteract the main rotor torque, but the corresponding feedback gain disappears. Results are illustrated with an example of yaw rate response in Fig. 11. The first two rows of plots show that with the nominal control gains $[\mathbf{Q} = 10^{-2}\ \mathrm{diag}(1, 1, 1, 40, 60, 25, 20, 20, 100, 1, 1, 2)]$ the SDRE exhibits better phase margin than the LQR. The LQR yields worse oscillations even for small latencies. Breaking the main and tail rotor control coupling in the model significantly improves control performance with unaccounted latencies (see the third row of plots in Fig. 11). Higher unaccounted latencies dictate the necessity to reduce the control gains, which were achieved via reduction of the error cost matrix values from the nominal to $\mathbf{Q} = 10^{-2}\ \mathrm{diag}(0.1, 0.4, 0.4, 40, 20, 5, 4, 4, 8, 0.2, 0.2, 1)$. The lower gain design essentially blurs the difference between the SDRE and the LQR performance; however, higher latencies still show less oscillatory behavior of the SDRE (see the fourth row of plots in Fig. 11). The bottom row of plots demonstrates performance achievable by explicit inclusion of the latency into the control design via the state vector extension. It is worth noting that, compared with the case when the latency is explicitly taken into account in the system model, the low-gain design may appear either too conservative or as having insufficient stability margins and requires a number of trial-and-error attempts to achieve satisfactory results.

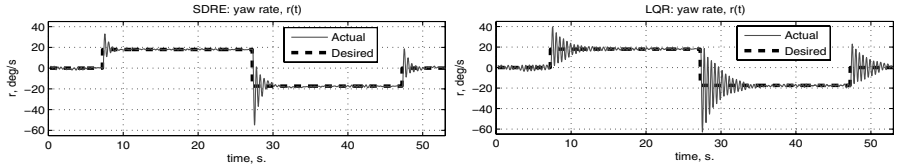

a) Three sample control delay; nominal design

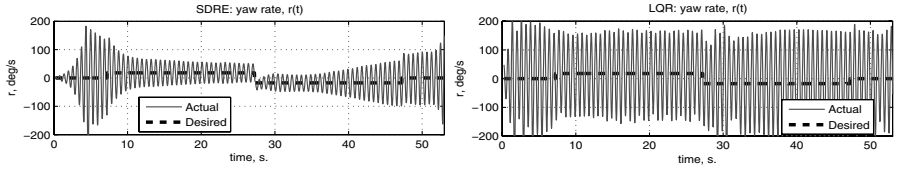

b) Five sample delay; nominal design

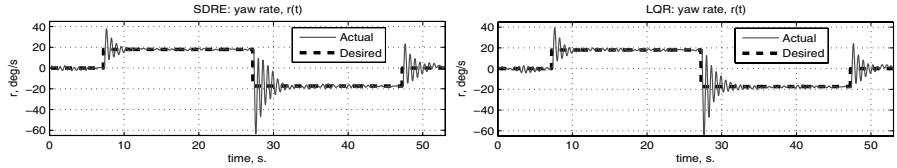

c) Five sample delay; decoupled main and tail rotor controls

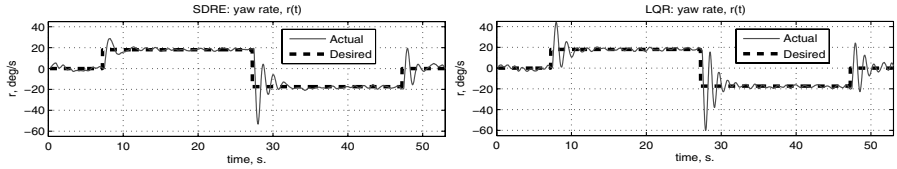

d) Ten sample delay; low control gains

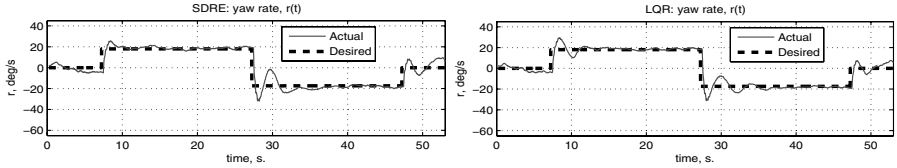

e) Ten sample delay; included in control design via the state vector

Fig. 11 Latency tests.

Flight Tests

We have demonstrated our work on a number of real flights using our XCell-90 model helicopter and the GATech GTMAX. Figure 12 illustrates an XCell-90 test flight: a 60×60 m square with 5 m/s desired speed. The actual flight trajectory differs from the desired due to wind presence and lower position control gains, as predicted by simulations when the wind information is unavailable. Nevertheless, altitude deviation from the desired never exceeded 2 m, which we consider satisfactory for a lightweight vehicle flying in windy conditions. The trajectory following can be improved by adding integral control on positions, as we did with the Yamaha GTMAX.

The GTMAX helicopter is a significantly heavier helicopter and, with added integral control on the x, y, and z state variables (and possibly different wind conditions at the time of the flight), is less affected by wind, as is seen from the Fig. 13. The plots demonstrate a similar flight pattern: 183×183 m square flown at 9 m/s. The maximum altitude error did not exceed 1.2 m, and the position error is less than 2 m. Although less sensitive to the wind and better built, controlling the actuators through the YACS results in a 180–200 ms delay in the control loop, which is equal to 9–10 control cycles. By decoupling yaw and main rotor collective control, and with slightly lowered bandwidth, the SDRE approach was robust enough to accommodate this without additional measures. On August 25, 2004, the augmented SDRE successfully performed during the Defense Advanced Research Projects Agency (DARPA) Software-Enabled Control program "Final Exam" at Fort Benning, Georgia. The demonstration flight included flying a pattern at 15.2 m/s around a test field [31].

The main purpose of these flight tests was to demonstrate feasibility of a real-time augmented SDRE flight control. Limited time and access to the vehicles and a number of hardware issues with our XCell-90 restricted our flight program to only a few tests and prevented us from flying more advanced trajectories.

Conclusions

In this work, we detailed the development of a SDRE controller for small helicopters. Clearly, the SDRE is more difficult to initially formulate than a LQR. However, once found, the actual implementation is straightforward. We further improved performance of the SDRE controller by introducing a nonlinear compensator that provides reference input and approximately cancels the mismatch between the vehicle dynamic model and its state-dependent coefficient parameterization. As shown by simulations, the combined control design provides significantly better performance than simply using a fixed trim control, which does not account for the vehicle dynamics. Simulations also demonstrate improved performance of the SDRE control as compared with the design based on a LQR. Robustness evaluation showed that the SDRE outperforms the LQR on more aggressive trajectories even when the model parameters are not known exactly. We found the state estimation errors to be the major factor in performance degradation. Although the SDRE demands more computational resources, the feasibility of a real-time implementation has been demonstrated with flight testing on the XCell-90 and Yamaha R-MAX (GTMAX) helicopters. Although we optimized the control approach for

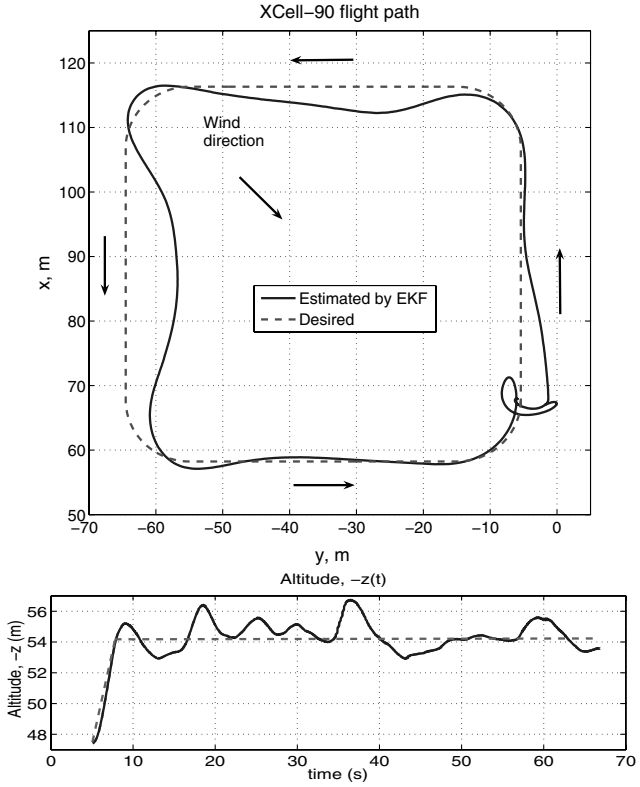

Fig. 12 XCell-90 flight test.

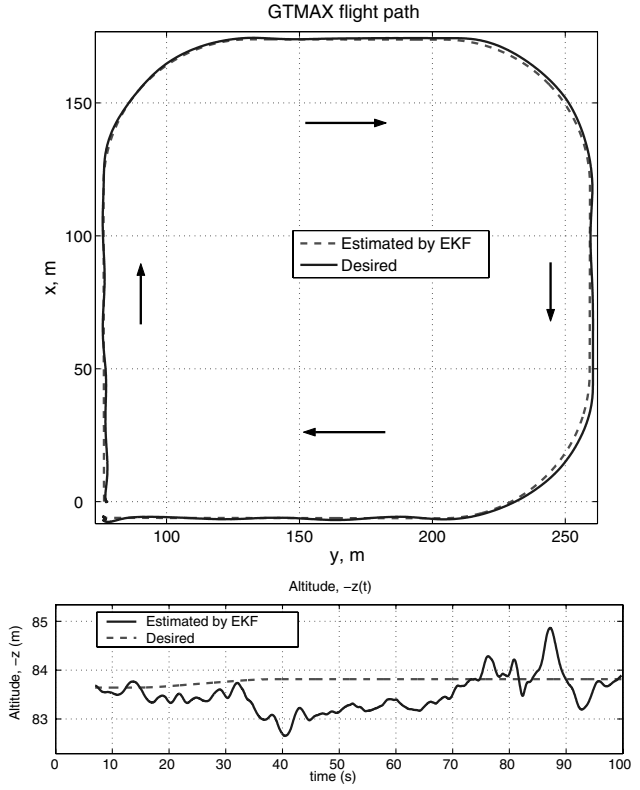

Fig. 13 GTMAX flight test.

small-scale vehicles, the equations developed can easily be generalized to a wide range of helicopter models.

Acknowledgments

This work was supported by the Defense Advanced Research Projects Agency Software-Enabled Control program under Contract No. F33615-98-C-3516 and the NSF Grant IIS-0313350. We deeply appreciate the Georgia Institute of Technology unmanned aerial vehicle team's help in making flight tests possible. We would also like to thank Geoff Harvey for software programming; Peter Haley, our radio control pilot; John Hunt, who provided hardware support; Jianmin He, who did the initial software work on the GTMAX implementation; and Richard Kieburtz for project management.

References

[1] La Civita, M., Papageorgiou, G., Messner, W. C., and Kanade, T., "Design and Flight Testing of a High-Bandwidth $\mathcal{H}_\infty$ Loop Shaping Controller for a Robotic Helicopter," *Proceedings of the AIAA Guidance, 33 Navigation, and Control Conference*, AIAA, Reston, VA, 2000; also AIAA Paper 2002-4836, Aug. 2002.

[2] Shim, H., Koo, T. J., Hoffmann, F., and Sastry, S., "A Comprehensive Study on Control Design of Autonomous Helicopter," *Proceedings of the IEEE Conference on Decision and Control*, Vol. 4, IEEE Publications, Piscataway, NJ, 1998, pp. 3653–3658.

[3] Johnson, E. N., and Kannan, S. K., "Adaptive Flight Control for an Autonomous Unmanned Helicopter," *AIAA Guidance, Navigation, and Control Conference*, AIAA, Reston, VA, Aug. 2002; also AIAA Paper 2002-4439.

[4] Cloutier, J. R., D'Souza, C. N., and Mracek, C. P., "Nonlinear Regulation and Nonlinear H-Infinity Control via the State-Dependent Riccati Equation Technique: Part 1, Theory," *Proceedings of the International Conference on Nonlinear Problems in Aviation and Aerospace*, University Press, Embry-Riddle Aeronautical University, Daytona Beach, FL, 1996, pp. 117–142.

[5] Shamma, J., and Cloutier, J., "Existence of SDRE Stabilizing Feedback," *IEEE Transactions on Automatic Control*, Vol. 48, No. 3, 2002, pp. 513–517.

[6] Cloutier, J. R., Stansbery, D. T., and Sznaier, M., "On the Recoverability of Nonlinear State Feedback Laws by Extended Linearization Control Techniques," *Proceedings of the American Control Conference*, Vol. 3, IEEE Publications, Piscataway, NJ, 1999, pp. 1515–1519.

[7] Curtis, J. W., and Beard, R. W., "Ensuring Stability of State-Dependent Riccati Equation Controllers via Satisficing," *Proceedings of the 41st IEEE Conference on Decision and Control*, Vol. 3, IEEE Publications, Piscataway, NJ, 2002, pp. 2645–2650.

[8] Hammett, K. D., Hall, C. D., and Ridgely, D. B., "Controllability Issues in Nonlinear State-Dependent Riccati Equation Control," *Journal of Guidance, Control, and Dynamics*, Vol. 21, No. 5, Sep.–Oct. 1998, pp. 767–773.

[9] Beeler, S. C., "State-Dependent Riccati Equation Regulation of Systems with State and Control Nonlinearities," NASA Langley Research Center, Tech. Rep. NASA/CR-2004-213245, National Institute of Aerospace, NIA 2004-08, Hampton, VA, July 2004.

[10] Banks, H. T., Lewis, B. M., and Tran, H. T., "Nonlinear Feedback Controllers and Compensators: A State-Dependent Riccati Equation Approach," North Carolina State University Tech. Rep. TR03-26, Center for Research in Scientific Computation, Raleigh, NC, July 2003.

[11] Parrish, D. K., and Ridgely, D. B., "Attitude Control of A Satellite using the SDRE Method," *Proceedings of the American Control Conference*, Vol. 2, IEEE Publications, Piscataway, NJ, June 1997, pp. 942–946.

[12] Stansbery, D. T., and Cloutier, J. R., "Position and Attitude Control of a Spacecraft using the State-Dependent Riccati Equation Technique," *Proceedings of the American Control Conference*, Vol. 3, IEEE Publications, Piscataway, NJ, 2000, pp. 1867–1871.

[13] Cloutier, J. R., and Stansbery, D. T., "Nonlinear, Hybrid Bank-to-Turn/Skid-to-Turn Missile Autopilot Design," *Proceedings of the AIAA Guidance, Navigation, and Control Conference*, AIAA, Reston, VA, 2001; also AIAA Paper 2001-4158.

[14] Menon, P. K., Lam, T., Crawford, L. S., and Cheng, V. H. L., "Real-Time Computational Methods for SDRE Nonlinear Control of Missiles," *Proceedings of American Control Conference*, Vol. 1, IEEE Publications, Piscataway, NJ, 2002, pp. 232–237.

[15] Menon, P. K., Iragavarapu, V. R., Sweriduk, G., and Ohlmeyer, E. J., "Software Tools for Nonlinear Missile Autopilot Design," *Proceedings of the AIAA Guidance, Navigation, and Control Conference*, AIAA, Washington, D.C., 1999; also AIAA Paper 1999-3975.

[16] Erdem, E. B., and Alleyne, A. G., "Experimental Real-Time SDRE Control of an Underactuated Robot," *Proceedings of the 40th IEEE Conference on Decision and Control*, Vol. 3, IEEE Publications, Piscataway, NJ, 2001, pp. 2986–2991.

[17] Bogdanov, A., "Optimal Control of a Double Inverted Pendulum on a Cart," Oregon Health and Science University, Tech. Rep. CSE-04-006, OGI School of Science and Engineering, Beaverton, OR, Dec. 2004.

[18] Wan, E. A., and Bogdanov, A. A., "Model Predictive Neural Control with Applications to a 6 DOF Helicopter Model," *Proceedings of American Control Conference*, Vol. 1, IEEE Publications, Piscataway, NJ, 2001, pp. 488–493.

[19] Gavrilets, V., Mettler, B., and Feron, E., "Nonlinear Model for a Small-Size Acrobatic Helicopter," *Proceedings of AIAA Guidance Navigation and Control Conference*, AIAA, Reston, VA, 2001; also AIAA Paper 2001-4333.

[20] Gavrilets, V., Shterenberg, A., Dahleh, M. A., and Feron, E., "Avionics System for a Small Unmanned Helicopter Performing Aggressive Maneuvers," *Proceedings of 19th Digital Avionics Systems Conference*, Vol. 1, IEEE Publications, Piscataway, NJ, 2000, pp. 1E2/1-1E2/7.

[21] Johnson, E., and Mishra, S., "Flight Simulation for the Development of an Experimental UAV," *Proceedings of the AIAA Modeling and Simulation Technology Conference*, AIAA, Reston, VA, Aug. 2002; also AIAA Paper 2002-4975.

[22] Slotine, J.-J. E., and Li, W., *Applied Nonlinear Control*, Prentice–Hall, Englewood Cliffs, NJ, 1991.

[23] Shamma, J., and Athans, M., "Analysis of Gain-Scheduled Control for Nonlinear Plants," *IEEE Transactions on Automatic Control*, Vol. 35, No. 8, 1990, pp. 898–907.

[24] Wu, F., "Control of Linear Parameter Varying Systems," Ph.D. Thesis, Dept. Mechanical Engineering, Univ. California, Berkeley, CA, 1997.

[25] Kleinman, D., "On an Iterative Technique for Riccati Equation Computation," *IEEE Transactions on Automatic Control*, Vol. 13, No. 1, 1968, pp. 114–115.

[26] Vidyasagar, M., *Nonlinear Systems Analysis*, 2nd ed., Prentice–Hall, Englewood Cliffs, NJ, 1993.

[27] Padfield, G. D., *Helicopter Flight Dynamics: The Theory and Application of Flying Qualities and Simulation Modeling*, AIAA, Reston, VA, 1996.

[28] Mettler, B., Gavrilets, V., Feron, E., and Kanade, T., "Dynamic Compensation for High-Bandwith Control of a Small-Scale Helicopter," *American Helicopter Society Specialist Meeting*, American Helicopter Society, Alexandria, VA, 2002.

[29] Marsden, J. E., and Tromba, A. J., *Vector Calculus*, W. H. Freeman, San Francisco, CA, 1981.

[30] van der Merwe, R., and Wan, E., "Sigma-Point Kalman Filters for Integrated Navigation," *Proceedings of the 60th Annual Meeting of The Institute of Navigation (ION)*, Institute of Navigation, Fairfax, VA, 2004, pp. 641–654.

[31] Johnson, E. N., Schrage, D. P., and Vachtsevanos, G., "Software Enabled Control Experiments with University-Operated Aircraft," AIAA Paper 2005-6956.